Available online at www.sciencedirect.com

ScienceDirect

Geochimica et Cosmochimica Acta 258 (2019) 156–173

Geochimica et Cosmochimica Acta

www.elsevier.com/locate/gca

Mechanism of solid-state clumped isotope reordering in carbonate minerals from aragonite heating experiments

Sang Chen [a,*], Uri Ryb [b,a], Alison M. Piasecki [a,c], Max K. Lloyd [a,d] Michael B. Baker [a], John M. Eiler [a]

[a] Division of Geological and Planetary Sciences, California Institute of Technology, Pasadena, CA 91125, United States
[b] Fredy and Nadine Herrmann Institute of Earth Sciences, The Hebrew University of Jerusalem, Jerusalem 9190401, Israel
[c] Department of Earth Science, University of Bergen, Bergen, Norway
[d] Department of Earth and Planetary Science, University of California, Berkeley, CA 94720, United States

Received 16 October 2018; accepted in revised form 13 May 2019; available online 22 May 2019

Abstract

The clumped isotope compositions of carbonate minerals are subject to alteration at elevated temperatures. Understanding the mechanism of solid-state reordering in carbonate minerals is important in our interpretations of past climates and the thermal history of rocks. The kinetics of solid-state isotope reordering has been previously studied through controlled heating experiments of calcite, dolomite and apatite. Here we further explore this issue through controlled heating experiments on aragonite. We find that Δ_{47} values generally decrease during heating of aragonite, but increase by 0.05–0.15‰ as aragonite starts to transform into calcite. We argue that this finding is consistent with the presence of an intermediate pool of immediately adjacent singly-substituted carbonate ion isotopologues ('pairs'), which back-react to form clumped isotopologues during aragonite to calcite transformation, revealing the existence of kinetically preferred isotope exchange pathways. Our results reinforce the 'reaction-diffusion' model as the mechanism for solid-state clumped isotope reordering in carbonate minerals. Our experiments also reveal that the reordering kinetics in aragonite is faster than in calcite and dolomite, making its clumped isotope composition highly susceptible to alteration during early diagenesis, even before conversion to calcite.

Keywords: Aragonite; Calcite; Clumped isotopes; Phase transition; Solid-state reordering; Reaction-diffusion model

1. INTRODUCTION

The carbonate 'clumped isotope thermometer' is based on the preferential bonding of ^{13}C and ^{18}O atoms within the same carbonate ion group at low temperatures, which transitions toward a more random isotope distribution among carbonate ions at high temperatures (Wang et al., 2004; Ghosh et al., 2006; Schauble et al., 2006; Eiler, 2011). Carbonate clumped isotope abundances are reported using the Δ_{47} notation, which is the ratio of the mass 47 isotopologue of CO_2 ($^{13}C^{18}O^{16}O$) to the mass 44 isotopologue ($^{12}C^{16}O_2$) in CO_2 released from a carbonate mineral by acid digestion, normalized to the ratio expected for a stochastic isotope distribution (Wang et al., 2004). The thermometer is interpreted to reflect homogeneous isotope exchange equilibrium between isotopic forms of carbonate ions in the mineral:

$$^{13}C\ ^{18}O\ ^{16}O_2^{2-} + {}^{12}C\ ^{16}O_3^{2-} \Longleftrightarrow {}^{12}C\ ^{18}O\ ^{16}O_2^{2-} + {}^{13}C\ ^{16}O_3^{2-} \quad (Rxn\ 1)$$

The temperature dependent equilibrium constant for this reaction can constrain the temperature of mineral formation or equilibration, independent of the carbon and/or

* Corresponding author.
E-mail address: scchen@caltech.edu (S. Chen).

https://doi.org/10.1016/j.gca.2019.05.018
0016-7037/

oxygen isotope composition of the fluid from which the mineral grew, and of the mineral itself (Eiler, 2007; Eiler, 2011). This quality makes this proxy useful for reconstructing Earth-surface temperatures for geological times and locations where the ^{18}O content of the water is not well known (e.g., Thiagarajan et al., 2014; Tripati et al., 2014; Rodríguez-Sanz et al., 2017; Henkes et al., 2018). Carbonate clumped isotope thermometry has also been used to infer temperatures of processes that occur in the shallow crust such as diagenesis (Dennis and Schrag, 2010; Huntington et al., 2011; Cummins et al., 2014; Winkelstern and Lohmann, 2016; Ryb and Eiler, 2018) and metamorphism (Ferry et al., 2011; Ryb et al., 2017; Lloyd et al. 2017).

The application of carbonate clumped isotope thermometry to the reconstruction of climate, water $\delta^{18}O$ values, or the thermal histories of rocks is complicated by the alteration of Δ_{47} values at elevated burial temperatures through solid-state reordering of C—O bonds (Passey and Henkes, 2012; Henkes et al., 2014; Stolper and Eiler 2015; Lloyd et al., 2017; Shenton et al., 2015; Gallagher et al., 2017; Lacroix and Niemi, 2019; Ryb et al., 2017; Ingalls, 2019). Previous studies have used controlled heating experiments to constrain the kinetics of solid-state isotope reordering of calcite (Passey and Henkes, 2012; Henkes, et al., 2014; Stolper and Eiler, 2015; Brenner et al., 2018), apatite (Stolper and Eiler, 2015) and dolomite (Lloyd et al., 2018). In these experiments, aliquots of the mineral of interest were held at a constant temperature for different amounts of time to create a time series over which the mineral Δ_{47} values could be observed to gradually approach equilibrium appropriate for that temperature. The rate of change of Δ_{47} values observed in such experiments constrains the kinetics of isotopic re-distribution among carbonate ions in the mineral lattice.

A key finding of these previous experiments is that solid-state alteration of Δ_{47} values in calcite, apatite, and dolomite all follow non-first-order kinetics. This finding has been interpreted as evidence that isotopic reordering is a two-stage process involving two mechanisms with different rate laws. Early in each set of time-series experiments, the rate of change of Δ_{47} values is dominated by a relatively fast process, which sharply transitions to a slower process that controls the remainder of the time series. Passey and Henkes (2012) attributed the initial rapid decrease in Δ_{47} in calcite to rapid diffusion facilitated by initially abundant lattice defects, and suggested the transition to slower kinetics reflects annealing of those defects, reducing their abundance and therefore the overall rate of isotopic re-equilibration. Stolper and Eiler (2015) proposed an alternative reaction-diffusion model to explain the two stages of calcite reordering. This model introduced the concept of 'pairs' and 'singletons'. Whereas a 'clump' is a carbonate group that contains both ^{13}C and ^{18}O, a 'pair' is a set of two adjacent carbonate groups, one of which contains ^{13}C and the other of which contains ^{18}O, while a 'singleton' is any carbonate group that contains either a single ^{13}C or a single ^{18}O, and has as immediate neighbors only carbonate ion units that lack ^{13}C and ^{18}O (i.e., they are all $^{12}C^{16}O_3^{2-}$). Stolper and Eiler (2015) suggested that clumped isotope evolution reflects rapid exchange between 'clumps' and 'pairs' coupled with slow diffusion-controlled separation of 'pairs' into isolated 'singletons' (Fig. 1a). In this case, the reordering reaction is described by the equation:

$$^{13}C\ ^{18}O\ ^{16}O_2^{2-} + {}^{12}C\ ^{16}O_3^{2-} \overset{k_f/k_b}{\Longleftrightarrow} pair \times \overset{k_d/k_s}{\Longleftrightarrow} {}^{12}C\ ^{18}O\ ^{16}O_{2,single}^{2-} + {}^{13}C\ ^{16}O_{3,single}^{2-} \quad (Rxn\ 2)$$

where k_f is the forward rate of transformation of a clump and neighboring unsubstituted carbonate ion into a pair, k_b is the rate of back reaction of a pair to form a clump, k_d is the diffusion-controlled rate of separation of pairs to form singletons, and k_s is the rate of diffusion for singletons to remake pairs.

The presence of the intermediate pool of pairs can explain the two stages of clumped isotope reordering as follows (Stolper and Eiler, 2015): The first stage of rapid reaction is dominated by the formation of pairs from clumps through isotope exchange of immediately adjacent neighbors, while the second stage is dominated by diffusion in the crystal lattice. Because the second stage is slower than the first, the region surrounding initial clumps become saturated with pairs of singly-substituted carbonate ion units that have not yet diffused away from each other; back reaction of this saturated pool of pairs is what buffers the decrease in the Δ_{47} value during the slower, diffusion-limited stage of the time series. Stolper and Eiler (2015) did not offer an atomistic explanation for why the transition from clump to pair is faster than the separation of pairs — intuition might predict these should have the same rate, as both types of reactions involve migration of ^{18}O (and perhaps ^{13}C) from one carbonate ion unit to another. This unresolved aspect of the reaction-diffusion model is one of the inspirations for the present study.

While both the defect-annealing and reaction-diffusion models have been successfully applied to natural samples (Henkes et al., 2014; Shenton et al., 2015; Lloyd et al., 2017; Ryb et al., 2017, Ingalls, 2019), it has been argued that the reaction-diffusion model is favored by the observation that the kinetics of isotopic reordering in optical calcite, brachiopods, and deformed and undeformed natural marbles are indistinguishable from one another (the idea being that these diverse materials might be expected to differ in their initial defect populations; Stolper and Eiler, 2015; Ryb et al., 2017; Lloyd et al., 2018). Nevertheless, there is a strong motivation to establish which of these two interpretations (or perhaps some other not yet proposed) is correct. And, if the reaction-diffusion model is correct, we still must understand why it is that an initial exchange between two adjacent carbonate ion groups is significantly faster than subsequent, but otherwise generally similar exchanges. The answers to these questions will dictate how carbonate clumped isotope measurements are used to reconstruct temperature-time histories of rocks that have been heated during protracted burial in sedimentary basins, and may inspire new tools based on the physical processes that control this phenomenon.

In this study, we re-examine this problem through observations of the kinetics of Δ_{47} changes when aragonite is exposed to elevated temperatures, at either high pressure

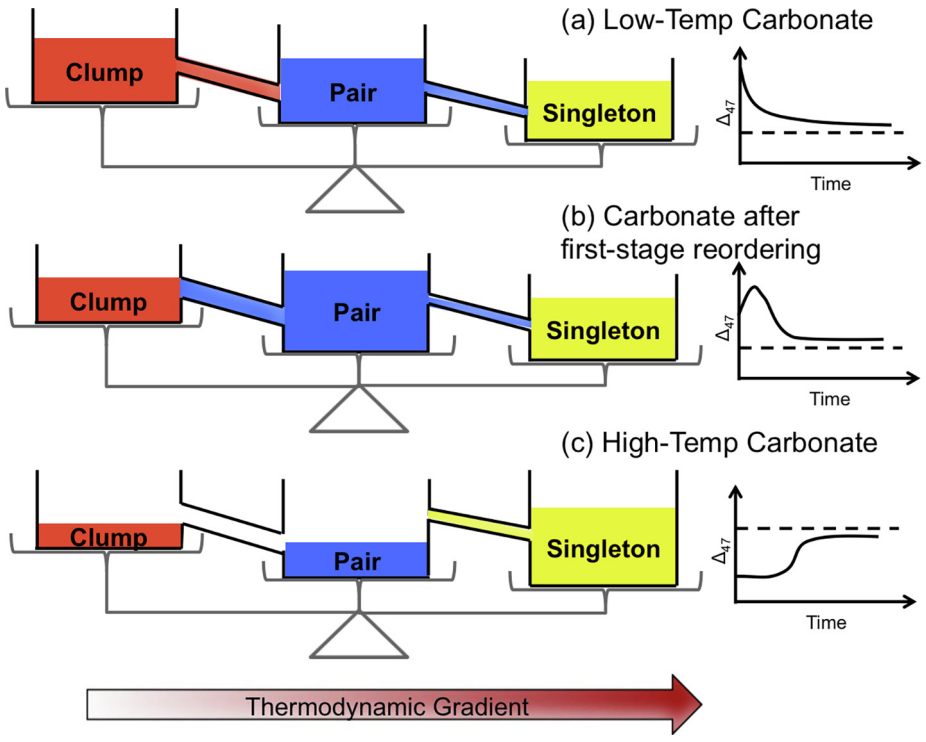

Fig. 1. A fluid flow analogy to the reaction-diffusion model as applied to different reordering experiments in this study. In the model, there are three pools of isotopically substituted carbonate groups in carbonate minerals: clumps, pairs and singletons, shown as fluids of different colors. The directions of the reactions (fluid flow) depend on two things: the fluid levels and the vertical positions of the tanks. The fluid level corresponds to actual concentrations of these carbonate groups, and the relative base height of the tanks corresponds to the thermodynamic trend. The plots on the right column show expected clumped isotope reordering patterns in a controlled heating experiment based on the abundance of clumps, pairs and singletons in each case. (a) This scenario represents a low-temperature carbonate, like the untreated starting material in the experiment. When exposed to high temperatures, the thermodynamic gradient drives the reaction from clumps to pairs and pairs diffuse away to form singletons, with a decrease in Δ_{47} over time. (b) This scenario represents a mineral that has been heated for a relatively short amount of time. In this case, pairs build up in the mineral at the expense of clumps. The pairs may diffuse to fill the singleton tank, but this process has a higher kinetic limit (thinner tube between blue and yellow), so that the build-up of pairs exceeds the formation of singletons. The pretreated calcite in our experiment may represent this scenario, with pairs building up in excess of equilibrium, and could remake clumps when a higher temperature is imposed. A similar scenario may explain Δ_{47} increases in aragonite as phase transition is triggered. The multi-stage reordering in aragonite is a likely combination of (a) and (b). An analogy for pair-excess created by phase transition may be a shrink in the size of the tank for pairs due to a rearrangement of carbonate ions in the lattices. The difference between the two minerals may also be related to different reaction rates (size of connection rubes), or different responses of the equilibrium pair concentration (vertical position of tanks) to the thermodynamic gradient. (c) This scenario represents the aragonite equilibrated at high temperatures. The equilibration process destroys most clumps and separates pairs into singletons, and the reordering reaction only goes in the reverse direction afterwards at a lower temperature. Clump formation can only happen when excess pairs build up, and a buffering time is expected for an increase in Δ_{47} to be observed. (For interpretation of the references to colour in this figure legend, the reader is referred to the web version of this article.)

where aragonite remains stable during heating, or at low pressure where it transforms into calcite over the time scales of our heating experiments. This work was initiated to obtain constraints on the susceptibility of aragonite to clumped-isotope reordering at shallow crustal conditions. However, our initial experimental results made it clear that this process provided an unexpected window on the atomistic mechanisms of the general phenomenon of clumped isotope reordering.

Aragonite is a polymorph of calcium carbonate that is common in nature, despite the fact that it is thermodynamically unstable at Earth surface conditions and readily transforms into calcite through heating or dissolution-reprecipitation reactions (Jamieson, 1953; Bischoff, 1969; Carlson, 1980; Budd, 1988). Clumped isotope compositions of aragonite follow the same temperature vs. Δ_{47} calibration curve as other carbonate minerals (Ghosh et al., 2006; Thiagarajan et al., 2011; Bonifacie et al., 2017). Clumped isotope compositions of fossil aragonite have been used in paleoclimate reconstructions of the recent ice age (Thiagarajan et al., 2014) and deeper times of the Phanerozoic (Dennis et al., 2013). Given its thermodynamic instability, it has generally been assumed that aragonite found in nature has been unaltered in its elemental and isotopic compositions. Recently, it has been shown in laboratory experiments and natural speleothems that the carbon, oxygen, and clumped isotope compositions can all be altered during the aragonite to calcite phase transition (Zhang

et al., 2014; Staudigel and Swart, 2016). In particular, Staudigel and Swart (2016) observed complicated clumped isotope reordering patterns in aragonite heating experiments over a range of temperatures (125–425 °C), including unexpected increases in Δ_{47} values during the heating process in certain experiments. These increases in Δ_{47} values are, however, not consistently observed in all their experiments, and are statistically indistinguishable from the previous time step in many cases. The authors noted these complexities but described aragonite reordering with a first order kinetic model. Staudigel and Swart (2016) also noticed that aragonite reordering initiates at lower temperatures than does calcite. However, a systematic decreasing trend in the bulk isotope composition (2.5‰ in $\delta^{18}O$ and 1.5‰ in $\delta^{13}C$) with time was observed in these experiments, suggesting a possible influence of open system exchange that would complicate the interpretation of these data as simply reflecting the solid-state reordering process.

We present new aragonite reordering experiments that reproduce and extend the previously observed complex clumped isotope reordering patterns, and we explain these findings as natural consequences of the reaction-diffusion model in a system undergoing a phase transition. We then test this hypothesis further through experiments in which we manipulate the distributions of clumped, pair, and singleton carbonate groups by preliminary thermal treatments to aragonite and calcite, and then observe the effect of those treatments on the solid-state reordering kinetics of both phases in a second heating experiment (Fig. 1b, c). We summarize our hypothesis and experimental tests in the reaction-diffusion framework with a fluid-flow analogy in Fig. 1, which are detailed in the following sections. Our experimental results suggest the presence of an intermediate pool of pairs in both aragonite and calcite, reenforcing the reaction-diffusion model of clumped isotope reordering.

2. MATERIALS AND METHODS

2.1. Aragonite samples

The aragonite used in our experiments was obtained from Tazouta, Sefrou Province, Fès-Boulemane, Morocco. It is a fist-sized aggregate of faceted intergrown crystals that are 0.5–1 cm in size. The sample was chosen due to its size, visual homogeneity and low-temperature origin. Replicate analysis ($n = 21$) of the bulk and clumped isotope composition of the aragonite yields a $\delta^{13}C$ value of 7.53 ± 0.17‰ (VPDB), a $\delta^{18}O$ value of -7.49 ± 0.19‰ (VPDB), and a Δ_{47} value of 0.757 ± 0.028‰ (means and aliquot-to-aliquot standard deviations; all reported Δ_{47} values are given in the absolute reference frame following Dennis et al., 2011). The Δ_{47} value corresponds to a formation temperature of 16 ± 5 °C (Dennis et al., 2011). The reported standard deviations of bulk and clumped isotope compositions are higher than the long-term reproducibility of carbonate standards at Caltech (0.03‰ for $\delta^{13}C$, 0.08% for $\delta^{18}O$, 0.02‰ for Δ_{47}), and suggest some natural heterogeneity within our sample. In interpreting our experiment results, we consider a measured isotope composition of a sample significantly different from others only when these differences exceed the internal variabilities in the starting materials.

2.2. Aragonite reordering experiments

The aragonite crystals were coarsely crushed into ~10 mg fragments (each ~1–2 mm across). The crystals were not further reduced in grain size because we wished to minimize the surface area and therefore any effects of adsorbed water or other surface chemistry. Approximately 20 mg of aragonite fragments were sealed in ¼″ quartz or Pyrex® tubes with 6.6 kPa isotopically distinct CO_2 gas ($\delta^{13}C = -11$‰, $\delta^{18}O = +16$‰, VPDB) in the headspace. The CO_2 gas was cryogenically purified with a dry ice-ethanol mixture to remove water vapor. The experiments were carried out under CO_2 atmosphere to minimize decarbonation of the aragonite, as well as to detect whether open-system isotope exchange reactions had occurred. The tubes containing aragonite and CO_2 were put into a box furnace held at one of several prescribed temperatures (200–500 °C). For each temperature, different aragonite samples were heated for different lengths of time to create a time series of clumped isotope reordering. After heating, we weighed each sample and determined the fractions of aragonite and calcite in the samples by X-ray diffraction (XRD) or Raman spectroscopy before isotope compositions were measured. For most samples, the weight loss is <0.3 mg before and after heating, and the bulk isotope compositions are within the initial heterogeneities of the starting material, consistent with no decarbonation or open-system exchange (Table 1, Fig. 2c, f). In three of the heating experiments, the aragonite was run in unsealed tubes and thus was exposed to the ambient atmosphere (Table 1). As with the sealed tube experiments, no significant decarbonation or open system exchange was observed for these three experiments. The aragonite to calcite phase transition was faster when exposed to the ambient atmosphere (Fig. 2b, e), but the clumped isotope reordering pattern was similar to the experiments with sealed tubes.

2.3. High-pressure aragonite experiment

For this experiment, we used a cylinder cored from a large crystal that comprised a portion of our aragonite sample. The core (260 mg) was loaded into a 0.2″ (outer diameter) Au capsule welded at both ends (for the second weld, the capsule was partially immersed in a water bath to minimize any heating of the aragonite). The capsule was run in a 1/2″ piston cylinder pressure vessel using an assembly that consisted of inner pieces of MgO (dried at 1000 °C for ~8 h), a straight-walled graphite furnace, and an outer sleeve of calcium fluoride. Temperature was monitored and controlled to within 1 °C of the set point using a $W_3Re/W_{25}Re$ thermocouple (care was taken to avoid thermocouple oxidation by bleeding N_2 gas into the slot in the thermocouple plate). Run conditions were 1.7 GPa and 600 °C and the sample was quenched after 10 days. Based on thermocouple output as a function of time, the sample cooled to room temperature in ~30 s. The experiment was

Table 1
Data from aragonite and calcite clumped isotope reordering experiments.

Sample	Temp (°C)	Heat time (hrs)	$\delta^{13}C$ (‰,VPDB)[e]	$\delta^{18}O$ (‰,VPDB)[e]	Calcite%[f]	Δ_{47} (‰,ARF)[g]
SC-A2[a]	500	0.71	7.055 ± 0.005	−7.665 ± 0.014	97	0.429 ± 0.015
SC-A3	500	0.33	7.548 ± 0.002	−7.022 ± 0.017	32	0.496 ± 0.016
SC-A4	500	0.17	7.308 ± 0.003	−7.518 ± 0.010	12	0.584 ± 0.020
SC-A5	500	0.50	7.668 ± 0.004	−7.050 ± 0.016	85	0.441 ± 0.019
SC-A6	500	0.20	7.014 ± 0.004	−7.283 ± 0.010	17	0.539 ± 0.010
SC-A7	500	1.05	6.996 ± 0.004	−7.674 ± 0.007	98	0.407 ± 0.018
SC-A8	500	0.08	7.016 ± 0.005	−7.583 ± 0.008	8	0.502 ± 0.017
SC-B1[a]	450	1	7.250 ± 0.003	−7.568 ± 0.004	13	0.564 ± 0.015
SC-B2	450	19	7.706 ± 0.002	−7.193 ± 0.009	70	0.473 ± 0.017
SC-B4	450	8.5	7.564 ± 0.003	−7.285 ± 0.009	75	0.499 ± 0.021
SC-B5	450	2	7.316 ± 0.002	−7.527 ± 0.009	24	0.528 ± 0.020
SC-B6	450	3.1	8.110 ± 0.002	−6.917 ± 0.006	7	0.551 ± 0.014
SC-B7	450	6.5	7.241 ± 0.004	−7.634 ± 0.008	92	0.340 ± 0.015
SC-B9	450	13.5	7.572 ± 0.004	−7.448 ± 0.009	91	0.485 ± 0.011
SC-B10	450	42	7.075 ± 0.005	−7.771 ± 0.004	100	0.317 ± 0.017
SC-B11	450	4	7.531 ± 0.003	−7.952 ± 0.008	13	0.504 ± 0.015
SC-B12	450	0.5	7.919 ± 0.003	−7.145 ± 0.006	11	0.655 ± 0.015
SC-B13	450	5	7.440 ± 0.003	−7.865 ± 0.010	64	0.385 ± 0.021
SC-B14	450	62	7.364 ± 0.003	−7.722 ± 0.007	100	0.334 ± 0.023
SC-B15	450	5.5	7.269 ± 0.003	−7.527 ± 0.013	85	0.366 ± 0.022
SC-C2[a,b]	350	5	7.585 ± 0.002	−7.370 ± 0.010	14	0.669 ± 0.023
SC-C3	350	13	7.494 ± 0.003	−7.655 ± 0.006	16	0.459 ± 0.013
SC-C4	350	1.02	7.268 ± 0.003	−7.453 ± 0.006	6	0.638 ± 0.013
SC-C5	350	3	6.985 ± 0.003	−7.727 ± 0.004	4	0.490 ± 0.018
SC-C6	350	18.5	7.728 ± 0.005	−7.341 ± 0.017	13	0.537 ± 0.018
SC-C7	350	37	7.696 ± 0.003	−7.268 ± 0.006	17	0.489 ± 0.016
SC-C8	350	45	7.153 ± 0.002	−7.616 ± 0.010	44	0.469 ± 0.017
SC-C9	350	24	7.389 ± 0.002	−6.976 ± 0.010	8	0.566 ± 0.014
SC-C10	350	72	7.150 ± 0.003	−7.696 ± 0.014	54	0.418 ± 0.022
SC-C11	350	9.5	7.105 ± 0.003	−7.397 ± 0.011	11	0.457 ± 0.019
SC-C12	350	100	7.707 ± 0.004	−7.220 ± 0.016	79	0.432 ± 0.019
SC-D1[b]	350	9	7.142 ± 0.008	−7.464 ± 0.012	6	0.559 ± 0.019
SC-D2	350	1	6.880 ± 0.007	−7.681 ± 0.011	3	0.563 ± 0.024
SC-D3	350	3	7.436 ± 0.010	−7.323 ± 0.014	4	0.696 ± 0.026
SC-D4b	350	18	7.697 ± 0.006	−6.942 ± 0.007	5	0.691 ± 0.020
SC-D5	350	0.5	7.400 ± 0.008	−7.449 ± 0.011	3	0.677 ± 0.030
SC-D6	350	48	7.613 ± 0.004	−6.845 ± 0.008	11	0.602 ± 0.016
SC-D7	350	72	7.064 ± 0.008	−7.202 ± 0.013	26	0.517 ± 0.025
SC-D8	350	6	7.306 ± 0.007	−7.489 ± 0.011	4	0.660 ± 0.028
SC-D8b	350	6	7.483 ± 0.006	−7.257 ± 0.008	4	0.643 ± 0.023
SC-D9	350	24	7.632 ± 0.007	−7.112 ± 0.011	8	0.681 ± 0.021
SC-D10	350	12	7.446 ± 0.004	−7.260 ± 0.007	4	0.596 ± 0.022
SC-E1	350	6	7.549 ± 0.004	−7.123 ± 0.005	3	0.628 ± 0.018
SC-E2	350	9	7.691 ± 0.010	−7.271 ± 0.004	2	0.665 ± 0.015
SC-E3	350	1	7.604 ± 0.002	−7.290 ± 0.004	2	0.698 ± 0.012
SC-E4	350	3	7.320 ± 0.002	−7.289 ± 0.005	2	0.718 ± 0.014
SC-E5	350	18	7.375 ± 0.002	−7.307 ± 0.006	5	0.711 ± 0.017
SC-E6	350	0.5	7.364 ± 0.003	−7.509 ± 0.006	1	0.688 ± 0.012
SC-E7	350	48	7.493 ± 0.005	−7.106 ± 0.004	4	0.618 ± 0.019
SC-E8	350	72	7.246 ± 0.002	−7.333 ± 0.003	5	0.593 ± 0.019
SC-E9	350	24	7.610 ± 0.004	−7.332 ± 0.007	5	0.647 ± 0.013
SC-E10	350	12	7.588 ± 0.004	−7.213 ± 0.003	4	0.680 ± 0.013
SC-H0[c]	350	0	7.428 ± 0.046	−7.122 ± 0.049	0	0.283 ± 0.016
SC-H1b	350	9	7.361 ± 0.004	−7.196 ± 0.005	6	0.317 ± 0.015
SC-H2b	350	72	7.445 ± 0.004	−7.201 ± 0.009	22	0.316 ± 0.022
SC-H3	350	48	7.639 ± 0.004	−7.029 ± 0.008	9	0.287 ± 0.019
SC-H4	350	1	7.477 ± 0.006	−7.062 ± 0.009	3	0.307 ± 0.020
SC-H5	350	18	7.459 ± 0.005	−7.077 ± 0.008	5	0.279 ± 0.019
SC-H6	350	0.5	7.495 ± 0.005	−6.981 ± 0.008	3	0.294 ± 0.020
SC-H7	350	12	7.388 ± 0.008	−7.153 ± 0.012	5	0.322 ± 0.020

(*continued on next page*)

Table 1 (*continued*)

Sample	Temp (°C)	Heat time (hrs)	$\delta^{13}C$ (‰,VPDB)[e]	$\delta^{18}O$ (‰,VPDB)[e]	Calcite%[f]	Δ_{47} (‰,ARF)[g]
SC-H8	350	3	7.551 ± 0.005	−7.077 ± 0.009	6	0.280 ± 0.019
SC-H9	350	6	7.499 ± 0.005	−7.023 ± 0.008	5	0.281 ± 0.019
SC-H10	350	24	7.440 ± 0.006	−7.006 ± 0.008	13	0.313 ± 0.010
AP-1	200	1	7.707 ± 0.004	−7.428 ± 0.012		0.656 ± 0.027
AP-7	200	18	7.461 ± 0.005	−6.834 ± 0.010		0.649 ± 0.027
AP-15	200	29	7.410 ± 0.004	−7.642 ± 0.008	0	0.661 ± 0.039
AP-C3	200	90	7.374 ± 0.002	−8.002 ± 0.005		0.709 ± 0.027
AP-C1	200	144	6.859 ± 0.003	−8.166 ± 0.004		0.723 ± 0.024
AP-4	300	1	7.233 ± 0.006	−7.928 ± 0.011	0	0.673 ± 0.033
AP-L	300	2	7.327 ± 0.004	−7.700 ± 0.010		0.635 ± 0.031
AP-2	300	13	7.392 ± 0.005	−7.240 ± 0.010	0	0.619 ± 0.041
AP-10	300	41	7.813 ± 0.004	−7.167 ± 0.010		0.720 ± 0.031
AP-D6	300	216	7.001 ± 0.003	−8.037 ± 0.006		0.693 ± 0.028
AP-G	400	1	7.096 ± 0.004	−7.568 ± 0.009	0	0.473 ± 0.009
AP-B4	400	2	6.135 ± 0.005	−7.055 ± 0.010	99	0.503 ± 0.033
AP-E	400	17	7.386 ± 0.004	−7.599 ± 0.006		0.608 ± 0.030
AP-B2	400	24.6	7.292 ± 0.005	−7.793 ± 0.011	1	0.586 ± 0.032
AP-B11	400	48	7.724 ± 0.007	−7.547 ± 0.015	94	0.549 ± 0.029
N21-1a1[d]	500	0	−1.381 ± 0.028	−16.788 ± 0.080	100	0.474 ± 0.015
N21-1a2	500	0	−1.168 ± 0.068	−16.894 ± 0.030	100	0.426 ± 0.017
N21-1b1	500	0.25	−1.658 ± 0.026	−17.205 ± 0.101	100	0.503 ± 0.018
N21-1b2	500	0.25	−2.296 ± 0.025	−16.641 ± 0.030	100	0.498 ± 0.008
N21-1c1	500	0.5	−1.592 ± 0.048	−17.049 ± 0.134	100	0.424 ± 0.014
N21-1c2	500	0.5	−1.802 ± 0.008	−16.705 ± 0.030	100	0.468 ± 0.007
N21-1d1	500	0.75	−1.879 ± 0.025	−16.936 ± 0.081	100	0.443 ± 0.019
N21-1d2	500	0.75	−1.391 ± 0.036	−17.176 ± 0.030	100	0.439 ± 0.001
N21-1e1	500	3	−1.549 ± 0.026	−16.860 ± 0.124	100	0.361 ± 0.012
N21-1e2	500	3	−2.394 ± 0.020	−16.803 ± 0.030	100	0.406 ± 0.011

[a] SC-A, SC-B and SC-C are unsealed heating experiments exposed to the ambient atmosphere.
[b] Both SC-C and SC-D experiments were conducted at 350 °C, and are labeled C-350 °C and D-350 °C in the figures.
[c] The SC-H series are reordering experiments with the clumped isotope randomized aragonite, H0 represents the composition after the 10-day high-pressure equilibration at 600 °C (average of 2 aliquots). The SC-H series and SC-D series were done at the same time under the same conditions.
[d] The N21-1 series are data from the two-step calcite reordering experiment. The experiment was replicated on two sets of samples. Samples N21-1a1 and N21-1a2 represent the composition after the first step of heating at 450 °C for 5 h.
[e] Reported as internal standard errors (1σ).
[f] Mass fraction of calcite was determined with XRD for AP samples, and with Raman spectroscopy for SC samples
[g] The Δ_{47} errors are total standard errors (1 SE) calculated following Daëron et al. (2016).

designed to equilibrate the clumped isotope composition (and potentially the concentration of pairs) at high temperature while maintaining aragonite in its stability field. The *P-T* conditions of the experiment were well within the aragonite field based on the $CaCO_3$ *P-T* phase relations compiled by Carlson (1980), and Raman spectroscopy showed that the post-run material was, indeed, aragonite (Fig. 3c). Next, an aliquot of this *P-T*-treated aragonite was measured for bulk and clumped isotope composition, while other fragments went through a reordering experiment at 350 °C at ambient pressure in a CO_2 atmosphere (see Section 2.2) before isotopic analysis. A 350 °C reordering experiment using untreated fragments of the aragonite was carried out in parallel for direct comparison.

2.4. Two-step calcite heating experiment

The two-step calcite heating experiment was designed to test if the complex clumped isotope reordering behavior in aragonite, in particular increases in Δ_{47} during heating, can occur in calcite. An optical calcite (catalog # N21-1) was selected from the Caltech mineral collection for its size, clarity, lack of visible defects or inclusions, and its relatively low-temperature origin. Bulk and clumped isotope analyses (n = 17) yield a $\delta^{13}C$ value of –1.55 ± 0.45‰ (VPDB), a $\delta^{18}O$ value of –16.96 ± 0.30‰ (VPDB) and a Δ_{47} value of 0.586 ± 0.006‰, which corresponds to a temperature of 63 ± 3 °C (Bonifacie et al., 2017). While the bulk isotope compositions of this calcite show substantial heterogeneity, the clumped isotope composition is relatively homogeneous. The sample was crushed into 10–30 mg fragments and sealed in quartz tubes with 6.6 kPa purified CO_2 gas that is isotopically distinct ($\delta^{13}C = –11‰$, $\delta^{18}O = +16‰$, VPDB) in the headspace. The tubes were initially heated at 450 °C for 5 h, and cooled quickly to room temperature (within ~2 min) using a compressed air duster. In the second step of this experiment, the pretreated samples from the first step were heated at 500 °C for different time intervals. We repeated this experiment twice to generate a replicate set of samples.

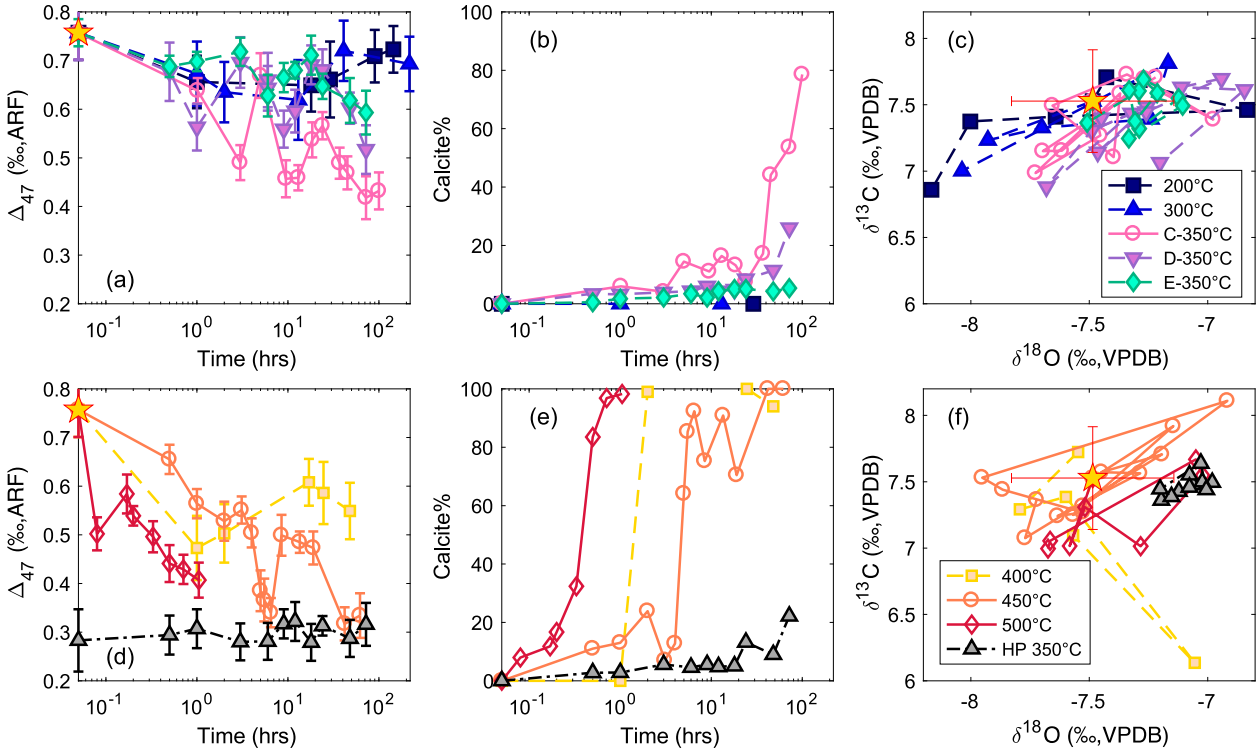

Fig. 2. Isotope and mineralogy data of the aragonite reordering experiments. Panels (a)-(c) show results of the ambient pressure experiments between 200 °C and 350 °C, while panels (d)-(f) show results of the ambient pressure experiments between 400 °C and 500 °C together with the 350 °C reordering experiment on the high pressure high temperature (600 °C) equilibrated aragonite. (a, d) Clumped isotope composition evolution with time (2SE error bars). The star represents the starting composition of the aragonite. At each temperature, increases in Δ_{47} values of 0.05–0.15‰ during the heating process are observed in the ambient pressure experiments. The black triangles represent the reordering experiment starting with clumped isotope randomized aragonite. Three heating experiments (C-350 °C, 450 °C, 500 °C) were conducted in air (open symbols) while others were conducted in CO_2 atmosphere (filled symbols). (b, e) Percentage of calcite in the samples determined by XRD (200 °C, 300 °C, 400 °C) or Raman spectroscopy (other experiments). There is scatter in the proportions of calcite from the XRD and Raman measurements, but in general there is an increase in calcite% with time in all experiments above 300 °C. (c, f) $\delta^{13}C$ and $\delta^{18}O$ values of the reordering experiments. The stars show the initial composition of the aragonite with 2σ standard deviations. The data points are connected in the order of heating time. Most data points scatter within the 2σ range of the initial composition of the aragonite ($\delta^{13}C = 7.53 \pm 0.17$‰ and $\delta^{18}O = -7.49 \pm 0.19$‰), and no systematic trend is observed, suggesting closed system behavior during the reordering experiments.

2.5. Mineralogy

In order to determine the extent to which aragonite transformed to calcite during the low-pressure, high-temperature experiments, samples were analyzed post-run by XRD or Raman spectroscopy. XRD measurements were performed with a Bruker D2 Phaser benchtop instrument (Cu K_α source) at Caltech. Relative peak areas at specific 2θ angles (30° for calcite, 46° for aragonite) were compared to determine the proportions of aragonite and calcite in the samples, using an approach similar to Dickinson and McGrath (2001). Relative peak areas were converted to mass fractions with a calibration curve generated from powder mixtures of pure aragonite and calcite. The detection limit of the method is approximately 1% for calcite and 5% for aragonite.

The Raman measurements were performed on a Renishaw M1000 Micro Raman Spectrometer at Caltech. The system uses a solid-state 514.3 nm laser with 100 mW beam power, and the measurements were done with 10% power at 5x magnification (~2 mW on sample) to minimize sample damage and maximize the covered area. Multiple spots (n = 5–10) were measured for each sample to get an average spectrum. Following Dickinson and McGrath (2001), the relative proportions of aragonite and calcite were determined using the scattering peaks for the carbonate ion planar bending mode (704 cm^{-1} for aragonite, 713 cm^{-1} for calcite). Relative peak areas were converted to mass fractions with a calibration constructed from powder mixtures of pure aragonite and calcite (Fig. 3). The peak areas scale close to 1:1 with mass fractions in the calibration standards. The Raman method was used for most samples because it requires less material than the XRD method we employed, and limited amounts of sample were recovered from each experiment (especially the high-pressure experiment described in Section 2.3). We also viewed the Raman measurement as more robust because of the greater linearity of its calibration trend.

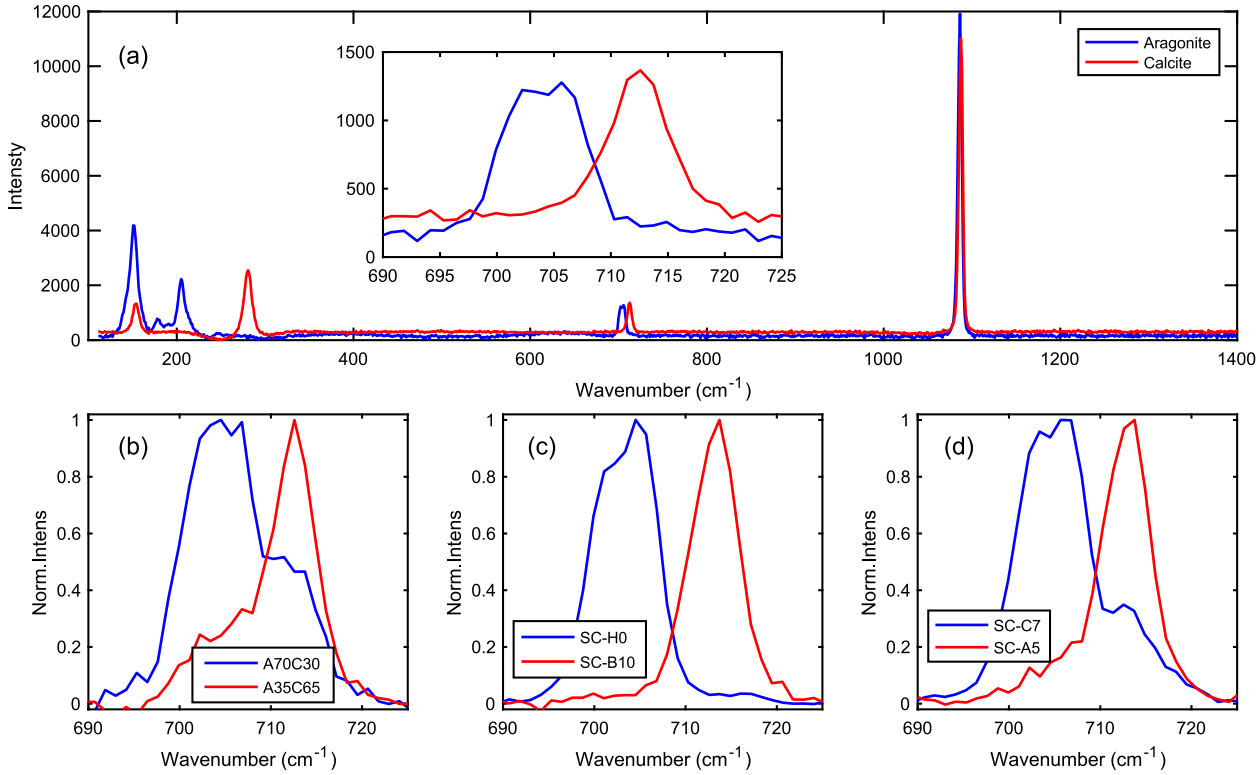

Fig. 3. Examples of Raman spectra used to determine fractions of aragonite and calcite in the samples. (a) Full spectra of pure aragonite (blue) and calcite (red), with the inset zooming in to the wavenumber range of carbonate ion planar bending mode, used to determine relative abundance of aragonite (704 cm^{-1}) and calcite (713 cm^{-1}) in the samples. (b) Spectra of powder mixtures of aragonite and calcite used as calibration standards. Examples shown here are a 70:30 aragonite:calcite mixture (blue) and a 35:65 aragonite:calcite mixture. (c) Spectra of samples from two experiments. SC-H0 is an aragonite sample whose clumped isotope composition was equilibrated at high temperature (600 °C) and high pressure (1.7 GPa). These P-T conditions preserved its aragonite structure. SC-B10 is a sample that has been completely converted to calcite after heating at 450 °C for 42 h. (d) Spectra of samples from two other experiments. SC-C7 was heated at 350 °C for 37 h, and was determined to have 17% calcite by peak area. SC-A5 was heated at 500 °C for 30 min, and has 85% calcite. (For interpretation of the references to colour in this figure legend, the reader is referred to the web version of this article.)

2.6. Stable isotope measurements

The bulk and clumped isotope compositions of the samples were measured using a Thermo MAT253 isotope ratio mass spectrometer at Caltech. Sample preparation and analysis procedures have been previously described in detail (Ghosh et al., 2006; Guo et al., 2009; Huntington et al., 2009; Passey et al., 2010). In brief, samples (~10 mg) were digested in phosphoric acid at 90 °C. Evolved CO_2 gas was purified cryogenically and went through a Porapak Q (50/80 mesh) GC column held at –20 °C, and then measured against a reference CO_2 gas. The measurements were standardized to heated (1000 °C) and water-equilibrated (25 °C) CO_2 gases, and in-house carbonate standards. In the calculation of bulk and clumped isotope compositions, we used the $^{17}O/^{16}O$, $^{18}O/^{16}O$ ratios for VSMOW and the $^{13}C/^{12}C$ ratio for VPDB suggested by Brand et al. (2010), which were found to minimize inter- and intra-laboratory discrepancies in reported Δ_{47} values (Schauer et al., 2016; Daëron et al., 2016). Measurements and uncertainties were calculated in the absolute reference frame (Dennis et al., 2011) following Daëron et al. (2016).

3. RESULTS

3.1. Aragonite-calcite phase transition

Given its instability under ambient pressure, aragonite is expected to transform into calcite during our low pressure heating experiments. XRD and Raman spectroscopy measurements confirm this general prediction, although there is significant variation in the reaction progress as a function of time (Fig. 2b, e). Similar variations in reaction progress were observed in the XRD powder patterns in the aragonite heating experiments of Staudigel and Swart (2016). This is likely related to the phase transition progressing inhomogeneously through the crystal lattice. Nevertheless, the overall pattern of the time and temperature evolution of the reaction is clear: At 200 and 300 °C, we observed negligible production of calcite over the course of our experiments. Significant amounts of newly grown calcite were observed at temperatures of 350 °C and above. When the samples were exposed to the ambient air (rather than being heated in a pure CO_2 atmosphere), 80% of the aragonite was converted to calcite in 72 h at 350 °C (Experiment SC-C). How-

ever, such rapid conversion at this relatively low temperature was atypical; the experiments conducted at 350 °C in a CO_2 atmosphere underwent 5–25% conversion after 72 h (Experiment SC-D, SC-E and SC-H). We conclude that when the reaction proceeds in air the phase transformation is accelerated, perhaps due to the presence of water vapor. At 400 °C and 450 °C, aragonite was mostly converted to calcite within 10 h. At 500 °C, nearly complete conversion to calcite was achieved in 40 min (Fig. 2e). Previous studies that conducted in-situ XRD and FTIR characterizations of the aragonite to calcite phase transition show a more rapid conversion over a period of ~10 min as the temperature is raised to 400–450 °C (Antao and Hassan, 2010; Koga et al., 2013). Other experimental studies have found timescales for the phase transition more similar to what we observe, from minutes to hours above 400 °C, depending on the sample origin, grain sizes and the experimental method (Davis and Adams, 1965; Madon and Gillet, 1984; Koga et al., 2013; Staudigel and Swart, 2016). Thus, we find a threshold temperature for significant phase transition similar to that observed in previous studies, and rates of conversion that lie at the slower end of the spectrum of values reported in previous work. We suspect that the relatively slow rate of the phase transition measured in our experiments is related to the length scale of the techniques we used to characterize crystal structure for most of our experimental products. XRD (used for only a few of our samples) observes structures that are coherent over hundreds to thousands of unit cells (10^{-8}–10^{-7} m), whereas Raman spectroscopy (used for most of our samples) observes structural properties at length scales corresponding to the wavelengths of infrared light (10^{-6} m). As a result, phase transitions detected by Raman spectroscopy might be seen to occur later than those detected by XRD (i.e., assuming phase transformation is structurally coherent over longer length scales as time progresses). This suspicion is supported by the observation that our XRD characterization of the phase transition at 400 °C indicated that it was completed in two hours, faster than the 450 °C experiment measured by Raman spectroscopy.

3.2. Clumped isotope reordering of low-temperature aragonite

Given the thermodynamic basis for the carbonate clumped isotope thermometer, it is expected that the Δ_{47} value of a carbonate mineral that initially grows at low-temperature and then is subjected to a higher temperature will monotonically decrease in Δ_{47} until it approaches the new, higher temperature equilibrium state of a lower Δ_{47} value (Fig. 1a). This behavior was previously observed in calcite, apatite, and dolomite reordering experiments

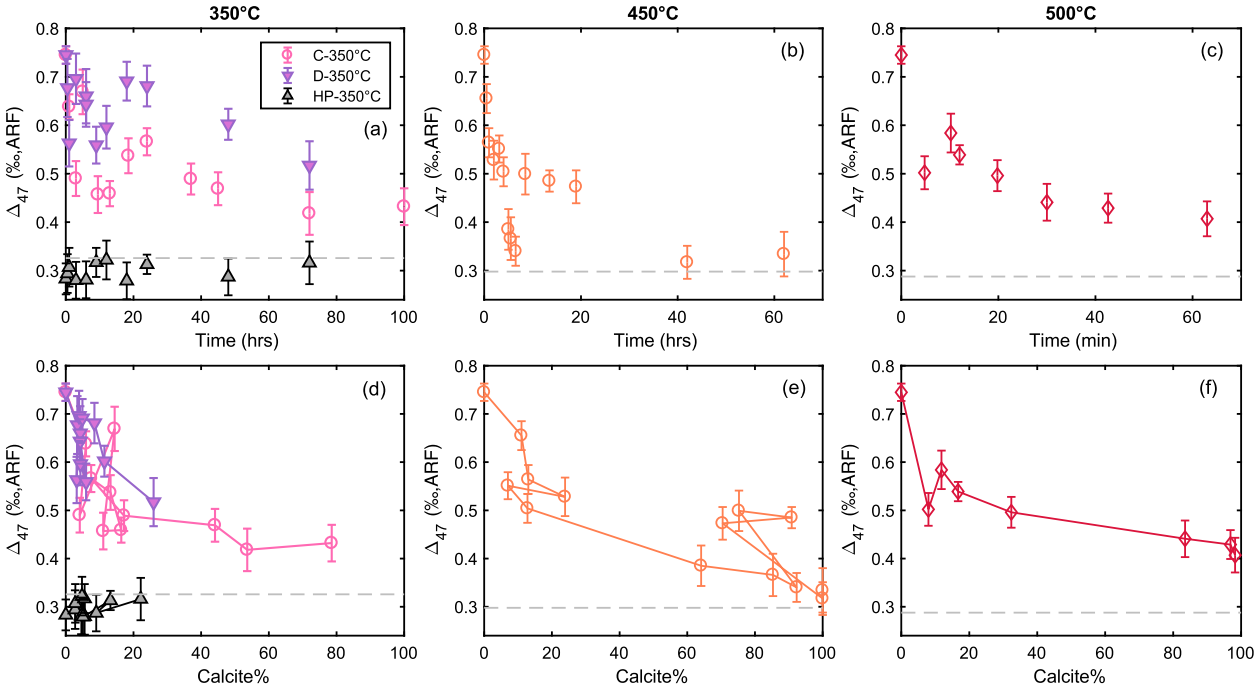

Fig. 4. Clumped isotope reordering paths with time (a-c) and percentage of calcite (d-f) in the sample for the experiments at 350 °C, 450 °C, and 500 °C. The lines in panels (d-f) connect points in the order of increasing running time. There are apparent reversals in calcite% with time in panels (d) and (e), which represent noise in the phase transition data at 350 °C and 450 °C. These reversals are more pronounced for experiments conducted in air (C-350 °C and 450 °C). Increases in Δ_{47} of 0.05–0.15‰ can be observed during each of the experiments, generally in the range of 0–20% phase transition. The experiments at 350 °C (C with ambient atmosphere, D and HP with CO_2 atmosphere) have slightly different magnitudes of Δ_{47} reordering with time, but the reordering paths are similar when calcite% is used as the x-axis, suggesting the reordering kinetics is related to the rate of phase transition. The gray triangles are reordering experiments at 350 °C with the clumped isotope randomized aragonite. The dashed lines mark the equilibrium Δ_{47} values at 350 °C, 450 °C ad 500 °C respectively (Bonifacie et al., 2017). Note that the x-axis for the 500 °C experiment in panel (c) is in minutes.

(Passey and Henkes, 2012; Henkes et al., 2014; Stolper and Eiler, 2015; Lloyd et al., 2018; Brenner et al., 2018). The reaction progress of solid-state isotopic reordering we observe in aragonite violates this expectation. Following an initial rapid decrease in Δ_{47}, we observe abrupt increases in Δ_{47}, with amplitudes in the range of 0.05–0.15 ‰, followed by a more gradual decrease in Δ_{47} values toward the thermodynamic equilibrium values (Fig. 2a, d, Fig. 4). This complex pattern has amplitudes of initial fall and subsequent rise that are large multiples of our analytical precision, and was observed to be significant and generally homologous in form in all of the experiments in which there was significant contrast between the initial and final equilibrium Δ_{47} values.

In our 350 °C experiments conducted in both air (SC-C) and CO_2 (SC-D and SC-E), it is clear that there are two separate increases in Δ_{47} in the first 24 hours, separated by an intermediate 'dip', and that both of the increases and all three periods of decrease are statistically well resolved (Figs. 2a, 4). There is a suggestion that the 450 °C experiment conducted in air could also have two separate periods of increasing Δ_{47}, but the first of them is not clearly resolved from the surrounding pattern of decreasing Δ_{47}. Experiments conducted at higher and lower temperatures have only one increase in Δ_{47} during the reordering process.

For most series of experiments conducted at one temperature, the first (or only) increase in Δ_{47} observed mid-way through the heating period occurred at the initial stage of the phase transition, i.e., the sample contained less than 20% calcite as determined by XRD or Raman spectroscopy (Fig. 4). However, as the proportion of calcite increases (i.e., >20%), the Δ_{47} values decrease again with further heating. Because the timing of the first appearance of calcite and time-evolution in the calcite/aragonite ratio are somewhat irregular in detail, it is not always clear how the rate and direction of change in Δ_{47} relates to the progress of the aragonite to calcite phase transition. However, when we plot the percentage of calcite vs. the Δ_{47} value (a bulk measurement of both aragonite and calcite), it is clear that increases in Δ_{47} occur early in the progress of the aragonite to calcite transition (Fig. 4). In summary, the reorganization of ^{13}C and ^{18}O (i.e., changes in Δ_{47} value) that occurs when aragonite is heated can be described as a (at least) three-stage process: initial destruction of $^{13}C—^{18}O$ bonds (decrease in Δ_{47}), followed by a re-formation of $^{13}C—^{18}O$ bonds (increase in Δ_{47}), followed by a monotonic decay in $^{13}C—^{18}O$ bonds until the high temperature equilibrium Δ_{47} value is reached. As noted above, in some experiments, a second cycle of increase and subsequent decrease in Δ_{47} is observed. The stage or stages of heating during which $^{13}C—^{18}O$ bonds re-form is both a strong departure from thermodynamic equilibrium at the conditions of the experiment, and clearly first occurs during the early stage of aragonite to calcite transition. This pattern is reproducible across a temperature range of more than 100 °C. We also note that the Δ_{47} values approach equilibrium at rates that are statistically indistinguishable from the calcite reordering experiments (Passey and Henkes, 2012; Henkes et al., 2014; Stolper and Eiler, 2015) after most of the aragonite has been converted to calcite.

3.3. Clumped isotope reordering of high-temperature-equilibrated aragonite

The aragonite heated at 600 °C at high-pressure for 10 days achieved a clumped isotope composition ($\Delta_{47} = 0.283 \pm 0.016$‰) that is within error of the expected equilibrium at 600 °C ($\Delta_{47\_eqm} = 0.273 \pm 0.021$‰, Bonifacie et al., 2017) (Note that $\delta^{13}C$ and $\delta^{18}O$ of this material are similar to other samples of the starting material: 7.43‰ and −7.12‰, VPDB, respectively; Fig. 2f). When this pretreated aragonite was subsequently subjected to a second stage of heating at 350 °C in a CO_2 atmosphere, the Δ_{47} increased slightly over the course of 72 h to the somewhat higher Δ_{47} value expected for equilibrium at 350 °C, accompanied by 22% conversion of aragonite to calcite (Fig. 2d, e, Fig. 4a, d). The amount of phase transition is similar to the untreated low-temperature aragonite going through the same reordering experiment, but we see no evidence for a sharp rise in Δ_{47} in the middle of the second heating period, as occurred when non-pre-treated aragonite was subjected to this same low-pressure heating schedule (Fig. 4a, d). A key feature of the high P-T treatment performed on this sample is that it involved a time-at-temperature sufficiently prolonged such that the reaction-diffusion model would predict complete mutual equilibration of all three populations of isotopic species: clumps, pairs and singletons (Fig. 1c). This series of experiments demonstrates that the anomalous rise in Δ_{47} associated with conversion of aragonite to calcite does not occur in materials that have already attained a fully equilibrated high-temperature isotopic structure due to a long, high-temperature 'soak'; that is, this phenomenon requires that the aragonite to calcite transition takes place in a material that has experienced a sharp drop in Δ_{47} within the previous few hours. This finding also indicates that the increase in Δ_{47} does not arise through a kinetic isotope effect associated with the aragonite to calcite transition (i.e., a dependence of the rate of phase transition on the isotopic composition of the carbonate groups).

3.4. Clumped isotope reordering in a two-step calcite experiment

After we subjected two samples of calcite to a first heating treatment of 450 °C for 5 h, their Δ_{47} values dropped from 0.586‰ to 0.474‰ and 0.426‰, respectively, without significant changes in their bulk $\delta^{13}C$ or $\delta^{18}O$ (Table 1, Fig. 5). When each of these pre-heated calcites were subjected to a second heat treatment at 500 °C, their Δ_{47} values increased by 0.03–0.06‰ in the first 15 min of the second heating treatment, before decreasing again afterwards. Interpretation of this experiment must be equivocal as the variations in Δ_{47} that we observe are near the 2 standard error limit of significance. Nevertheless, both experimental series suggest that it is possible to subject calcite to a heating schedule that creates subtle but resolvable increases in Δ_{47} in the absence of a phase transition. The specific heating schedule we selected to create this effect was based on a prediction of the reaction-diffusion model, and this experiment is important to our efforts below to interpret and generalize

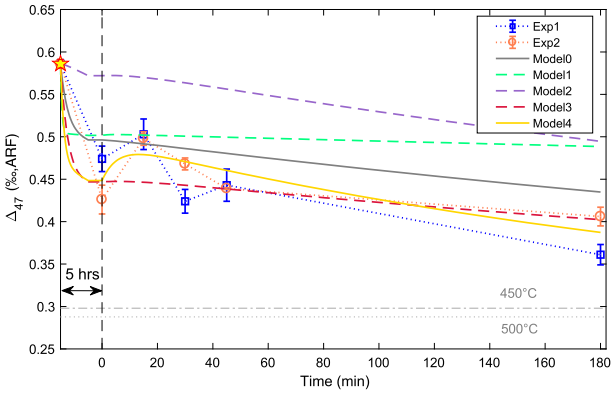

Fig. 5. Clumped isotope reordering in the two-step calcite heating experiment compared to model calculations from the reaction-diffusion model (Stolper and Eiler, 2015). The squares and circles (connected by dotted lines) are replicate reordering experiments at 500 °C (second step), to the calcite that was pretreated by heating at 450 °C for 5 h (first step). The star marks the initial composition of the calcite. The vertical line separates the two steps. To the left of the line is the Δ_{47} change with the pretreatment at 450 °C for 5 h (time is not to scale with the second step on the x-axis). The Δ_{47} value at time zero represents the composition after the pretreatment. The dash-dot and dotted horizontal lines mark the thermodynamic equilibrium values at 450 °C and 500 °C (Bonifacie et al., 2017). In both 500 °C reordering experiments, the Δ_{47} values increased by 0.03–0.06‰ after 15 min of the second stage, before decreasing toward equilibrium. The solid and dashed curves are model outputs from the reaction-diffusion model with different parameter combinations. The model parameters for each case are listed in Table 2. Significant changes to the original model parameters in Stolper and Eiler (2015) are required to generate a curve that fits the data with a well-resolved Δ_{47} increase at the beginning of the second stage (solid gold curve).

the more pronounced Δ_{47} increases we observe during the aragonite to calcite transition.

4. DISCUSSION

The formation of excess $^{13}C—^{18}O$ bonds (producing an increase in Δ_{47}) during high-temperature transformation of aragonite to calcite is a significant, reproducible observation of this study and appears to act opposite to thermodynamic driving forces. Yet it also is not a kinetic isotope effect associated with some elementary step of the phase transformation, as no such isotopic reordering is observed when aragonite is allowed to achieve a fully equilibrated high-temperature isotopic structure prior to transformation to calcite. This phenomenon has not only been reproduced in our experiments, but also resembles the similar (though less regular) findings of previous heating experiments performed on aragonites of different origins (Staudigel and Swart, 2016). Moreover, we see suggestive evidence that the same phenomenon can be made to occur in calcite, absent any phase transformation, provided the calcite is subjected to a specific heating schedule. We find no evidence that any of these effects are accompanied by changes in bulk isotopic content ($\delta^{13}C$ and $\delta^{18}O$) that might provide evidence for open system reactions. We suggest that this behavior is an integral feature of solid-state isotopic reordering in carbonate minerals that needs to be incorporated in future reordering models.

In the following discussion, we describe how this behavior can be conceptually explained by the reaction-diffusion model of Stolper and Eiler (2015). We also discuss the new insights these findings provide regarding the kinetics of atomic mobility within carbonates and the kinetics of the aragonite to calcite transition. Finally, we use these results to support the presence and significance of pairs in carbonate minerals, and to generalize the reaction-diffusion mechanism across carbonate minerals

4.1. The reaction-diffusion model and high-temperature formation of Excess $^{13}C—^{18}O$ Bonds

Increases in Δ_{47} during a high-temperature heating step are a previously unrecognized prediction of the reaction-diffusion model of Stolper and Eiler (2015). Specifically, we now recognize that this phenomenon is a natural consequence of the fact that disproportionation of clumps to form pairs leads to a brief period of time (typically hours at the temperatures of our experiments) when the pairs have not yet diffused apart to form singletons and have the potential to back-react to re-form clumps (Fig. 1b).

Stolper and Eiler (2015) proposed the reaction-diffusion model as a way of explaining the kink in the time evolution of decreasing Δ_{47} values; specifically, they suggested that this feature marks the time when the rate of net formation of pairs by breakdown of clumps is nearly balanced by the rate of diffusive separation of pairs to form singletons.

We observe several low-pressure time-series where Δ_{47} values rise sharply during the aragonite to calcite transition, with amplitudes of 0.13–0.18‰, or roughly 30–40% of the contrast between the initial Δ_{47} value and the Δ_{47} value the carbonate would have after fully equilibrating at the temperature of the experiment. Interpreted in the context of the reaction-diffusion model, this implies that the reaction of a clump to form a pair largely reverses at the onset of the aragonite to calcite transition (i.e., 50–80% of clumps destroyed during the earliest stage of heating temporarily re-form). For experiments with two separate Δ_{47} increases at 350 °C, the second increase is almost a quantitative reversal of the previous drop in Δ_{47}.

Perhaps the strongest argument that an intermediate pool of pairs is required to drive Δ_{47} increases at high temperature comes from the lack of a Δ_{47} rise when aragonite is given a long, very high temperature, high pressure 'soak' before the aragonite to calcite transition (see Section 3.3 above). This experiment indicates that the sharp increases in Δ_{47} are only a feature of aragonite that undergoes transformation to calcite immediately (within minutes to hours) after its Δ_{47} has decreased in response to heating.

This can be understood as a consequence of the pair mechanism: For all of our experiments involving a single, low-pressure stage of heating, clumps are transformed to pairs early in the experiment, but those pairs have not had enough time to diffusively separate to form singletons, so they are present as a potentially reactive pool of excess pairs when the phase transformation occurs (Fig. 1b). In

aragonite that has undergone long, high-temperature, high-pressure heating, the pool of pairs has been depleted through diffusion to form singletons, removing that pool of excess pairs (Fig. 1c).

We hypothesize that the reformation of clumps from an over-abundant pool of pairs is associated with the rearrangement of carbonate ions in the crystal lattice on the unit-cell scale. Several models have been proposed to describe the atomistic mechanism of the aragonite-calcite phase transition. Previous studies agree that this solid-state transition involves displacement of calcium layers relative to carbonate layers, and 30° rotations of carbonate groups (Madon and Gillet, 1984; Antao and Hassan, 2010; Miyake and Kawano, 2010). The rotation of carbonate groups converts the 9-coordinated aragonite structure to the 6-coordinated calcite structure, and clearly involves reorganization of Ca—O bonds (Madon and Gillet, 1984; Miyake and Kawano, 2010). However, prior studies did not specify whether this reorganization of the geometries of carbonate ions is accomplished by the breaking and re-forming of C—O bonds or simply involves motions of carbonate ions with respect to one another. Our findings that the aragonite-to-calcite reaction is accompanied by a large change in $^{13}C—^{18}O$ ordering suggests that the first possibility is the case.

Each O atom in the aragonite lattice has up to eight nearest neighbor O atoms (i.e., those that can be reached in a straight line, omitting those that share the moving atom's own carbonate ion unit, and noting that some sites that are 'adjacent' by this definition are much closer than others; Fig. 6a). Thus, if the clump-to-pair transition involved purely random movement of O atoms from one

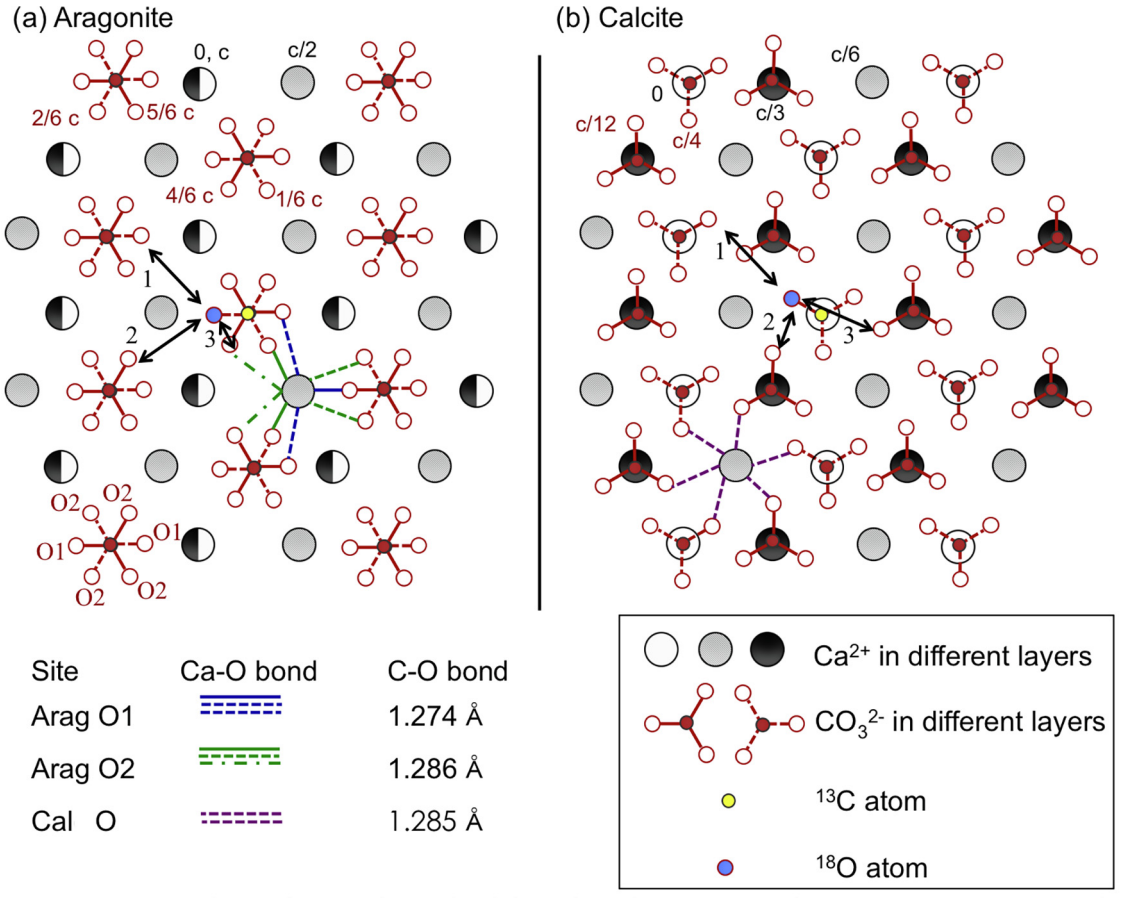

Fig. 6. Comparison of aragonite and calcite mineral structures. The structures are presented as projections along the c-axis of the minerals, modified from Madon and Gillet (1984). The positions of Ca^{2+} and CO_3^{2-} along the c-axis are marked in the top two rows of the projected structures. The half filled Ca^{2+} ions in (a) represent overlapping layers at position 0 and c along the c-axis. The ^{18}O and ^{13}C atoms are marked by a different color, and are bonded here as a clumped isotopologue. The blue, green and purple lines show the Ca—O bond in the minerals. While all Ca—O bonds in calcite are equivalent, there are five different Ca—O bonds in the 9-coordinated aragonite structure, which gives rise to two non-equivalent oxygen sites O1 and O2. The length of the C—O bonds associated with O1 and O2 sites are listed in the lower left portion of the figure. O1 is more loosely bonded to Ca^{2+} with a slightly stronger C—O bond. In panel (a), the double headed arrows show 3 different pathways for possible preferential oxygen exchange that involve breaking the fewest and weakest bonds. Pathway 1 is an O1-O1 exchange, while pathways 2 and 3 are O1-O2 exchange. In panel (b), the arrows show the same exchange pathways as in (a) after the mineral structure is rearranged. The O1-O2 exchange pathways in (a) have pairs remaining in neighboring positions after the phase transition in (b), and may cause the Δ_{47} increases observed during phase transition by a forced back-exchange.

carbonate ion unit to a randomly-selected neighbor, and that the aragonite to calcite transition was accompanied by a second random exchange of an O atom with one of its set of possible 'straight line' nearest neighbors, it should only be possible to recover a small fraction of the original clumped isotope signature (i.e., most ^{18}O atoms that make the first jump away from a clump will not return to their original carbonate ion unit on their second jump; nor are they likely to reach another ^{13}C atom on making a second jump). The fact that most of the Δ_{47} signature that was initially lost is recovered suggests that the transition from clumps to pairs preferentially involves O exchange between only one (or perhaps two) of the possible nearest neighbor pairs, and that the aragonite to calcite transformation is accompanied by an O exchange that takes advantage of that same preferred oxygen site or sites. This might be expected if one of the possible pathways for exchanging an O atom between two carbonate groups has a lower activation energy than any of the other possible exchange mechanisms, and so occurs at a higher rate. In the 9-coordiated aragonite structure, there are five different Ca—O bonds and two non-equivalent oxygen sites, O1 and O2 (Fig. 6a; Antao and Hassan, 2010; Ye et al., 2012). The strengths of the Ca—O and C—O bonds for these two oxygen sites are different, which we anticipate could give rise to different activation energies of the various possible oxygen exchange pathways. In particular, the three exchange pathways labeled in Fig. 6a involve breaking the weakest bonds in the aragonite structure and, we suggest, could be energetically favorable. Two of these three pathways involve an O1—O2 exchange (pathways 2 and 3 in Fig. 6a). After exchange through these two pathways, the aragonite-calcite phase transition would keep the singly-substituted carbonate groups in neighboring positions (i.e., remaining as pairs) as shown in Fig. 6b. We suggest that quantitative conversion of pairs to clumps can be explained as a two-step mechanism: (1) initial preferential conversion of clumps to pairs along the O1—O2 exchange pathway, followed by (2) forced exchange of O1—O2 oxygen atoms during the aragonite to calcite phase transition. This hypothesis is an attractive target for future molecular dynamic models of the kinetics of the $CaCO_3$ phase transition and solid-state clumped isotope reordering.

We also draw attention to the fact that the rise in Δ_{47} that accompanies the aragonite to calcite transition is observed at approximately the time when XRD or Raman evidence for calcite formation is first observed, but well before complete conversion of aragonite to calcite (by which time Δ_{47} has fallen again). It would be rational to argue that this is just the behavior expected if the rise in Δ_{47} reflects a kinetic isotope effect associated with the transition (i.e., a dependence of its rate on the isotopic content of the reacting carbonate ions). However, our experiment performed on aragonite that had been isotopically equilibrated at high pressure shows this is not the case. Isotope exchange between adjacent carbonate ion units happens over atomic length scales (10^{-10} m), whereas XRD and Raman observe structures that are coherent over much longer length scales (10^{-8}–10^{-6} m). A comparison of the apparent rates of these three measurements of the aragonite to calcite transition at different spatial scales is shown in an Arrhenius plot (Fig. 7). We see that over our experimental temperature range the rate of initial clump-to-pair conversion in aragonite is faster by an order of magnitude than the rate of XRD determined phase transition, which is in turn an order of magnitude faster than the rate of phase transition estimated by Raman spectroscopy over our experimental temperature range. We suggest that the structural rearrangements involved in the aragonite to calcite transition begin at short length scales and only gradually does the calcite structure become coherent to longer length scales; furthermore, we argue that the clumped isotope composition is sensitive to the earliest, shortest length scale re-arrangements, while XRD and Raman are sensitive to structural re-organization on increasingly longer length scales.

The trend in Fig. 7 for the rate of clumped isotope reordering in aragonite is not a straight line. This observation suggests that clumped isotope reordering may occur through two or more separate steps that differ in activation

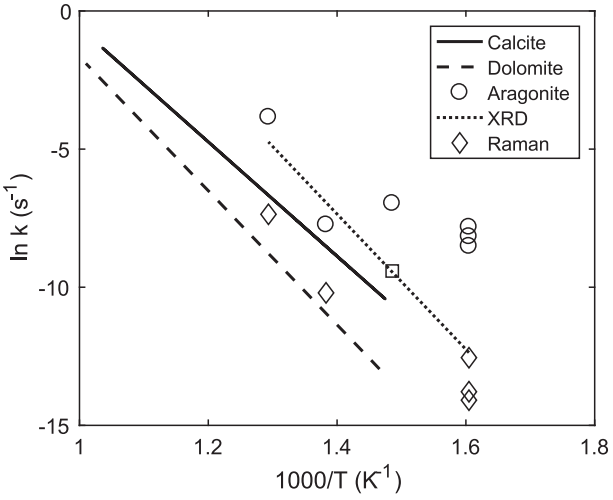

Fig. 7. Arrhenius plot of clumped isotope reordering and $CaCO_3$ phase transition kinetics. The solid and dashed line represents the rate constants of clump to pair conversion (k_f in Rxn 2) calculated from calcite (Stolper and Eiler, 2015) and dolomite (Lloyd et al., 2018) reordering experiments. The circles represent rate constants (k_f) for aragonite estimated by fitting the first stage of Δ_{47} decrease (before the first Δ_{47} increase as phase transition in triggered) in the experimental data with the reaction-diffusion framework. Clumped isotope reordering in aragonite is faster than calcite and dolomite. The dotted line represents rates of aragonite-calcite phase transition at 1 atm calculated from XRD measurements by Davis and Adams (1965). The estimated rate of phase transition measured by XRD in our 400 °C experiment (square) is consistent with the literature values. The diamonds represent rates of phase transition measured by Raman spectroscopy in our experiments. Detection of the phase transition by Raman spectroscopy postdates XRD measurements, and the rate of the aragonite to calcite transition as determined using either method is slower than the rate of the clumped isotope reordering reactions in aragonite. The rate constants for phase transition are estimated by $k = 1/\tau$, where τ is the e-folding time (63.2% reaction progress) of the transition. An exponential curve was fit to the noisy reaction progress data to estimate the rate of phase transition.

energies. This finding may offer insight into why we sometimes see two separate rises in Δ_{47} over the course of the aragonite to calcite transition. The two separate increases in Δ_{47} at 350 °C may reflect the fact that we can see two separate steps in a complex bond reordering process because the phase transition is slow, letting us observe isotopic evolution over a gradually spreading conversion of aragonite to calcite; by this interpretation, no clear evidence for two Δ_{47} rises is seen at higher temperatures simply because the phase transition progresses too quickly relative to our sampling interval.

In summary, we explain the complex evolution in Δ_{47} values observed when an aragonite that formed at low temperature converts to calcite at high temperature as an interplay between the mechanisms of isotope exchange between clumps, pairs and singletons on one hand and the dynamics of the aragonite-calcite phase transition on the other. The initial reduction in Δ_{47} that occurs when aragonite is first heated but has not yet reacted to form detectable calcite is an exchange between the clumped and unsubstituted carbonate ions to build up pairs in the aragonite lattice. This initial exchange preferentially occurs by an exchange of oxygen between only one (or perhaps two) of the several possible pairs of nearest-neighbor O sites. The subsequent rise in Δ_{47} marks the first detectable stage of conversion of aragonite to calcite, which is associated not only with re-alignment of carbonate ion units but also with the breaking and re-forming of C—O bonds. The first of these bond breaking and re-forming events take advantage of the same low activation energy pathway that is the preferred mechanism of clumped isotope reordering. Thus, the O atom exchange that is forced by the phase transition effectively reverses any immediately preceding conversion of clumps to pairs. The only exception to this pattern is seen when aragonite is allowed to isotopically equilibrate at high temperatures before conversion to calcite, which we take as evidence for slower diffusion-limited separation of pairs to form randomly distributed singletons. We suggest that the observation of two separate periods of increasing Δ_{47} when low-temperature aragonite is converted to calcite at 350 °C indicates that this structural re-organization occurs through two or more steps that differ in their rates, but that are only clearly observed when phase transformation is slow yet goes to completion (conditions that are not both met at significantly higher or lower temperatures).

4.2. Back-reaction of pairs during sharp temperature changes

Our two-step calcite heating experiments were designed to generate pair excesses and drive back-reactions to reform clumps in the absence of a phase transformation (Fig. 1b). During the first stage of the experiments, the samples were heated at 450 °C for 5 h. According to the kinetic parameters derived in Stolper and Eiler (2015), these temperature-time conditions should have allowed the clumps-to-pairs reaction to go nearly to completion. In contrast, the diffusion-limited separation of pairs to form singletons should not yet have progressed to a significant extent. Thus, a pair excess should have existed at this point. The samples were then exposed to a higher temperature of 500 °C, which lowers the equilibrium pair concentration, increasing the driving force for pairs to either separate or back-react to form clumps.

The magnitude of the change in Δ_{47} predicted by the reaction-diffusion model for this heating history depends on the excesses above a random distribution for both clumps and pairs prior to any heating (i.e., when the studied sample first crystallized), and the temperature dependence of the equilibrium concentrations for clumps and pairs. These quantities are relatively well known for the clumped isotope species, but are essentially unverified assumptions in the case of pairs. If we adopt the assumed values by Stolper and Eiler (2015) for pairs, and adjust their estimated values for the rate constants, k_f, k_d in Rxn 2 within their stated uncertainties, the model can predict a rise in Δ_{47} during the second stage of this heating experiment (Model-1 in Fig. 5) that is similar in timing to the rises we observe, but so muted in amplitude it could not be measured with current analytical methods (whereas we reproducibly observe an effect several times analytical precision). We constructed several alternative model predictions of the consequences of our experimental heating schedule by increasing the temperature sensitivity of the pair excess by a factor of 6 relative to the value assumed by Stolper and Eiler (2015) (Model-4 in Fig. 5). A model that closely matches the rate of Δ_{47} decrease in this experiment also requires adjustment of the initial pair concentration, by a few parts in 10^4 (see Table 2 and Fig. 5). These modifications demonstrate the capacity of the reaction-diffusion model to generate temporary increases in Δ_{47}, but show that quantitatively fitting experimental data requires tuning the parameters that define the abundances and behavior of pairs—parameters that are, at present, poorly constrained. For this reason we consider this set of experiments and the calculations discussed above to provide only suggestive evidence regarding the underlying mechanism that produces the anomalous Δ_{47} rises in calcite during the two-stage heating process.

Despite the complexities in and assumptions of the model required to explain the significant Δ_{47} increases, the experimental observations are important for two reasons: (1) they show that anomalous increases in Δ_{47} can occur during heating in the absence of a phase transformation; and (2) they confirm a peculiar prediction of the reaction-diffusion model that arises from the hypothesized existence and properties of pairs. It remains true that we have no direct observations of pairs (nor can we think of a way in which they could be observed with meaningful precision). However, these results suggest that the dynamics of interconversion of clumps, pairs and singletons could be universal to the solid-state isotopic reordering of carbonate minerals (and perhaps other molecular salts).

We could not think of a way that the defect-annealing mechanism would be predicted to drive a Δ_{47} increase during heating, against the thermodynamic driving force. Our expectation is that the defect density in a crystal changes the rate of diffusion and thus the time it takes to reach equilibrium, but not the direction of clumped isotope evolution. We observed Δ_{47} reversals against thermodynamic trends in both the aragonite-calcite phase transition and the two-

Table 2
A summary of two-stage calcite reordering models in Fig. 5.

Model	Tuned variable[a]	Variable Value relative to original model[b]	Timing of 2nd-stage Δ_{47} increase (min)	Magnitude of Δ_{47} increase (‰)
0	None	Original	N/A	None
1	(k_f, k_d)	(2, 0.5)	5	0.001
2	A	1.6	3	0.0003
3	(A, d_i)	(1.6, 0.99985)	6	0.0005
4	(A, d_i, k_f, k_d)	(6, 0.99918, 2, 2)	13	0.03

[a] For the tuned variables, k_f and k_d represent the rate constants for isotope exchange in Rxn 2. 'A' represents the temperature sensitivity of the equilibrium pair concentration presented in the reaction-diffusion model of Stolper and Eiler (2015), following the equation: $\ln[pair]_{eqm}(T)/[pair]_{random} = A/T$. The variable '$d_i$' represents an additional variable introduced to account for potential differences in initial pair concentrations of different calcite minerals, and to better fit the data of the first-stage of reordering in our experiment. In Model-3 and Model-4, $[pair]_{initial} = d_i[pair]_{eqm}$.
[b] Values represent a multiplication factor applied to the original reaction-diffusion model parameters.

stage calcite heating experiments. While the former may involve creation of new defects as the crystal structure is rearranged, we do not expect significant changes in the number of defects in the same calcite over a short period of time (15 min) as the temperature is raised by 50 °C. Only the presence of an intermediate pool of pairs can possibly cause the observed clumped isotope reversals.

We also note that the observed Δ_{47} increases in calcite are expected only for specific heating pathways, have been observed only for the experiments discussed here, and are of secondary importance to the overall reordering trend. The original pair-diffusion model parameters in Stolper and Eiler (2015) still predict the general trend of our calcite data better than the variety of other parameters that generate Δ_{47} increases (Fig. 5), as well as for calcite under a wide range of experimental and geological thermal histories.

4.3. Differences between aragonite and calcite in reordering kinetics

While the reaction-diffusion reordering mechanism can conceptually explain the complicated clumped isotope reordering pattern in aragonite, it should be noted that the kinetics of clumped isotope reordering in aragonite are distinct from calcite, even in the absence of the aragonite to calcite phase transformation. In our experiments, aragonite clumped isotope reordering is triggered at temperatures much lower than those for calcite. No clumped isotope reordering was observed for calcite up to temperatures of 380 °C (Passey and Henkes, 2012; Stolper and Eiler, 2015). In contrast, we see aragonite reordering take place at temperatures as low as 200 °C in our experiments, and significant reordering has been observed at even lower temperatures (125–175 °C) by others (Staudigel and Swart, 2016). Given the complicated reordering pathways and the interplay with the phase transformation, it is challenging to estimate accurate rate constants for clumped isotope reordering in aragonite with the existing data. Using the reaction-diffusion model to fit the data, the initial stage of rapid Δ_{47} decrease by clump-pair conversion in aragonite requires a rate constant (k_f in Rxn 2) that is 1–2 orders of magnitude larger than that in calcite (Fig. 7). Large uncertainties remain with these estimates due to the scarcity of data points before the phase transition is triggered to cause a reversal in Δ_{47}. We expect time series experiments of aragonite reordering at high pressure (in its stability field) to provide better estimates of the rate constants. However, it is a robust observation in our experiments that when an aragonite-calcite phase transition is involved, the time it takes for the mineral to reach clumped isotope equilibrium is much shorter than for calcite (Fig. 4). For example, it took 500 h for calcite to reach equilibrium at 430 °C (Stolper and Eiler, 2015), while the equilibrium composition was reached in 42 h in our 450 °C experiment as aragonite was converted to calcite (Fig. 4). As a result, aragonite's initial clumped isotope composition is predicted to alter at much lower temperatures than that of calcite and dolomite (Stolper and Eiler, 2015; Lloyd et al., 2018), making it highly susceptible to moderate heating during early diagenesis. The Δ_{47} increases during heating and phase transition may further complicate the interpretation of clumped isotope compositions of aragonite and aragonite-derived calcite in sedimentary basin settings. Because unit-cell-scale transformations of aragonite to calcite can artificially raise Δ_{47} values, carbonate materials with 'cold' clumped isotope temperatures that appear to be pristine, unmodified aragonite (based on XRD and Raman spectroscopy) may be indistinguishable from aragonite that experienced moderate heating, partially-reordered in the solid-state, and partially transformed to calcite at a scale finer than the above conventional techniques can detect. However, our reordering experiments make it possible to better constrain a quantitative model of clumped isotope reordering in carbonate minerals in general, and potentially will allow a more complete understanding of the temperature history of natural carbonates measured using clumped isotopes.

Because aragonite and calcite have the same chemical composition, the difference in reordering kinetics is likely a result of structural differences between the two minerals. We surmise that the rate of isotope exchange in the solid-state is determined by the bonding environment of atoms in the crystal lattice. Aragonite has a more tightly compacted structure compared to calcite, and the shortest pathway between oxygen atoms in neighboring carbonate groups is smaller in aragonite than in calcite. Nevertheless,

certain Ca—O and C—O bonds in aragonite are longer and thus weaker in aragonite than in calcite (Antao and Hassan, 2010; Ye et al., 2012). As a result, the pairs in aragonite that originate from disproportionation of a clump may have a lower energetic barrier to form (and to exchange back to the clumped species, in the event that a phase transformation forces an oxygen exchange between neighboring pairs). The bonding environment of oxygen atoms is also less symmetric in aragonite than calcite (Fig. 6), which may create multiple pools of pairs at the non-equivalent oxygen sites; we speculate that this diversity of O bonding environments may be related to the fact that we observe two separate Δ_{47} increases when the aragonite to calcite transformation occurs at 350 °C. The factors controlling these elementary kinetic steps could be further investigated by performing reordering experiments of other carbonate minerals of both calcite-type (e.g., siderite, rhodochrosite) and aragonite-type (e.g., strontianite, witherite) structures, as well as developing molecular dynamic models of solid-state isotope exchange.

5. CONCLUSIONS

We conducted a series of isotopic reordering experiments in aragonite at different temperatures and observed complicated patterns of decreasing and increasing Δ_{47} values. In general, the reordering pathway can be described as a series of steps in which Δ_{47} initially drops sharply, then rises sharply at the onset of conversion of aragonite to calcite, and finally falls asymptotically toward the high-temperature equilibrium value. We propose that this pattern can be explained with the reaction-diffusion reordering mechanism associated with the aragonite-calcite phase transition. We tested the hypothesis with a reordering experiment on an aragonite sample whose isotopic structure (clumps, pairs and singletons) was equilibrated at high temperature and pressure. The lack of an abrupt rise in Δ_{47} when this sample was subsequently converted to calcite suggests that such Δ_{47} increases require pools of excess pairs. We further tested the presence of pairs in carbonates in general by conducting a two-step calcite heating experiment. After a pretreatment aimed at increasing pair concentrations in calcite, a small but statistically significant rise in Δ_{47} was reproduced during the second stage of the experiment. These experiments suggest a general mechanism of clumped isotope reordering based on the reaction-diffusion model that can be applied to different carbonate minerals.

Although the mechanism of clumped isotope reordering in aragonite and calcite may be similar, the kinetics of the reordering reactions is different for the two minerals. Clumped isotope compositions of aragonite are highly susceptible to reordering at moderate heating, and the reordering kinetics is much faster than in calcite and dolomite. This must be taken into account when applying the clumped isotope thermometer to natural aragonite that has gone through early diagenesis. The lower activation energy of clumped isotope reordering in aragonite as compared to calcite may be related to the bonding environment of the oxygen atoms in the crystal lattice associated with its structure. Factors determining the kinetics of isotope exchange in carbonate minerals could be further investigated by reordering experiments of other carbonate minerals, as well as molecular dynamic models of the mobility of different isotopes through crystal structures.

ACKNOWLEDGMENTS

We thank George Rossman for help with Raman spectroscopy and providing calcite samples. The XRD measurements were performed in Nathan Lewis's lab at Caltech. We thank Alex Lipp for help with the calcite reordering experiments. S.C. would like to acknowledge financial support from China Scholarship Council for Ph.D. study at Caltech. This work was supported by NSF EAR Award #1322058 to J.M.E.

APPENDIX A. SUPPLEMENTARY MATERIAL

Supplementary data to this article can be found online at https://doi.org/10.1016/j.gca.2019.05.018.

REFERENCES

Antao S. M. and Hassan I. (2010) Temperature dependence of the structural parameters in the transformation of aragonite to calcite, as determined from in situ synchrotron powder X-Ray-diffraction data. *Can. Mineralog.* **48**(5), 1225–1236. https://doi.org/10.3749/canmin.48.5.1225.

Bischoff J. L. (1969) Temperature controls on aragonite-calcite transformation in aqueous solution. *Am. Mineral.* **54**, 149–155.

Bonifacie M., Calmels D., Eiler J. M., Horita J., Chaduteau C., Vasconcelos C., Agrinier P., Katz A., Passey B. H., Ferry J. M. and Bourrand J.-J. (2017) Calibration of the dolomite clumped isotope thermometer from 25 to 350 °C, and implications for a universal calibration for all (Ca, Mg, Fe)CO_3 carbonates. *Geochim. Cosmochim. Acta* **200**, 255–279. https://doi.org/10.1016/j.gca.2016.11.028.

Brand W. A., Assonov S. S. and Coplen T. B. (2010) Correction for the 17O interference in δ(13C) measurements when analyzing CO_2 with stable isotope mass spectrometry (IUPAC Technical Report). *Pure Appl. Chem.* **82**, 1719–1733. https://doi.org/10.1351/pac-rep-09-01-05.

Brenner D. C., Passey B. H. and Stolper D. A. (2018) Influence of water on clumped-isotope bond reordering kinetics in calcite. *Geochim. Cosmochim. Acta* **224**, 42–63. https://doi.org/10.1016/j.gca.2017.12.026.

Budd D. A. (1988) Aragonite-to-calcite transformation during fresh-water diagenesis of carbonates: Insights from pore-water chemistry. *GSA Bulletin* **100**(8), 1260–1270. https://doi.org/10.1130/0016-7606(1988)100<1260:ATCTDF>2.3.CO;2.

Carlson W. D. (1980) The calcite-aragonite equilibrium: effects of Sr substituion and anion orientational disorder. *Am. Mineral.* **65**, 1252–1262.

Cummins R. C., Finnegan S., Fike D. A., Eiler J. M. and Fischer W. W. (2014) Carbonate clumped isotope constraints on Silurian ocean temperature and seawater δ18O. *Geochim. Cosmochim. Acta* **140**, 241–258. https://doi.org/10.1016/j.gca.2014.05.024.

Daëron M., Blamart D., Peral M. and Affek H. P. (2016) Absolute isotopic abundance ratios and the accuracy of Δ47 measurements. *Chem. Geol.* **442**, 83–96. https://doi.org/10.1016/j.chemgeo.2016.08.014.

Davis B. L. and Adams L. H. (1965) Kinetics of the calcite ⇌ aragonite transformation. *J. Geophys. Res.* **70**(2), 433–441. https://doi.org/10.1029/JZ070i002p00433.

Dennis Kate J., Affek H. P., Passey B. H., Schrag D. P. and Eiler J. M. (2011) Defining an absolute reference frame for 'clumped' isotope studies of CO_2. *Geochim. Cosmochim. Acta* **75**(22), 7117–7131. https://doi.org/10.1016/j.gca.2011.09.025.

Dennis Kate J. and Schrag D. P. (2010) Clumped isotope thermometry of carbonatites as an indicator of diagenetic alteration. *Geochim. Cosmochim. Acta* **74**(14), 4110–4122. https://doi.org/10.1016/j.gca.2010.04.005.

Dennis K. J., Cochran J. K., Landman N. H. and Schrag D. P. (2013) The climate of the Late Cretaceous: New insights from the application of the carbonate clumped isotope thermometer to Western Interior Seaway macrofossil. *Earth Planet. Sci. Lett.* **362**, 51–65. https://doi.org/10.1016/j.epsl.2012.11.036.

Dickinson S. R. and McGrath K. M. (2001) Quantitative determination of binary and tertiary calcium carbonate mixtures using powder X-ray diffraction. *Analyst* **126**(7), 1118–1121. https://doi.org/10.1039/b103004n.

Eiler J. M. (2007) "Clumped-isotope" geochemistry—The study of naturally-occurring, multiply-substituted isotopologues. *Earth Planet. Sci. Lett.* **262**(3), 309–327. https://doi.org/10.1016/j.epsl.2007.08.020.

Eiler J. M. (2011) Paleoclimate reconstruction using carbonate clumped isotope thermometry. *Quat. Sci. Rev.* **30**(25), 3575–3588. https://doi.org/10.1016/j.quascirev.2011.09.001.

Ferry J. M., Passey B. H., Vasconcelos C. and Eiler J. M. (2011) Formation of dolomite at 40–80 °C in the Latemar carbonate buildup, Dolomites, Italy, from clumped isotope thermometry. *Geology* **39**(6), 571–574. https://doi.org/10.1130/G31845.1.

Gallagher T. M., Sheldon N. D., Mauk J. L., Petersen S. V., Gueneli N. and Brocks J. J. (2017) Constraining the thermal history of the North American Midcontinent Rift System using carbonate clumped isotopes and organic thermal maturity indices. *Precambr. Res.* **294**, 53–66. https://doi.org/10.1016/j.precamres.2017.03.022.

Ghosh P., Adkins J., Affek H., Balta B., Guo W., Schauble E. A., Schrag D. and Eiler J. M. (2006) ^{13}C–^{18}O bonds in carbonate minerals: A new kind of paleothermometer. *Geochim. Cosmochim. Acta* **70**(6), 1439–1456. https://doi.org/10.1016/j.gca.2005.11.014.

Guo W., Mosenfelder J. L., Goddard W. A. and Eiler J. M. (2009) Isotopic fractionations associated with phosphoric acid digestion of carbonate minerals: Insights from first-principles theoretical modeling and clumped isotope measurements. *Geochim. Cosmochim. Acta* **73**(24), 7203–7225. https://doi.org/10.1016/j.gca.2009.05.071.

Henkes G. A., Passey B. H., Grossman E. L., Shenton B. J., Pérez-Huerta A. and Yancey T. E. (2014) Temperature limits for preservation of primary calcite clumped isotope paleotemperatures. *Geochim. Cosmochim. Acta* **139**, 362–382. https://doi.org/10.1016/j.gca.2014.04.040.

Henkes G. A., Passey B. H., Grossman E. L., Shenton B. J., Yancey T. E. and Pérez-Huerta A. (2018) Temperature evolution and the oxygen isotope composition of Phanerozoic oceans from carbonate clumped isotope thermometry. *Earth Planet. Sci. Lett.* **490**, 40–50. https://doi.org/10.1016/j.epsl.2018.02.001.

Huntington K. W., Eiler J. M., Affek H. P., Guo W., Bonifacie M., Yeung L. Y. and Came R. (2009) Methods and limitations of 'clumped' CO_2 isotope (Δ_{47}) analysis by gas-source isotope ratio mass spectrometry. *J. Mass Spectrom.* **44**(9), 1318–1329. https://doi.org/10.1002/jms.1614.

Huntington, Katharine W., Budd D. A., Wernicke B. P. and Eiler J. M. (2011) Use of clumped-isotope thermometry to constrain the crystallization temperature of diagenetic calcite. *J. Sediment. Res.* **81**(9–10), 656–669.

Ingalls M. (2019) Reconstructing carbonate alteration histories in orogenic sedimentary basins: Xigaze forearc, southern Tibet. *Geochim. Cosmochim. Acta* **251**, 284–300. https://doi.org/10.1016/j.gca.2019.02.005.

Jamieson J. C. (1953) Phase equilibrium in the system calcite-aragonite. *J. Chem. Phys.* **21**(8), 1385–1390. https://doi.org/10.1063/1.1699228.

Koga N., Kasahara D. and Kimura T. (2013) Aragonite crystal growth and solid-state aragonite-calcite transformation: a physico-geometrical relationship via thermal dehydration of included water. *Cryst. Growth Des.* **13**(5), 2238–2246. https://doi.org/10.1021/cg400350w.

Lacroix B. and Niemi N. A. (2019) Investigating the effect of burial histories on the clumped isotope thermometer: An example from the Green River and Washakie Basins, Wyoming. *Geochim. Cosmochim. Acta* **247**, 40–58. https://doi.org/10.1016/j.gca.2018.12.016.

Lloyd M. K., Eiler J. M. and Nabelek P. I. (2017) Clumped isotope thermometry of calcite and dolomite in a contact metamorphic environment. *Geochim. Cosmochim. Acta* **197**, 323–344. https://doi.org/10.1016/j.gca.2016.10.037.

Lloyd M. K., Ryb U. and Eiler J. M. (2018) Experimental calibration of clumped isotope reordering in dolomite. *Geochim. Cosmochim. Acta* **242**, 1–20. https://doi.org/10.1016/j.gca.2018.08.036.

Madon M. and Gillet P. (1984) A theoretical approach to the kinetics of calcite ⇌ aragonite transition: application to laboratory experiments. *Earth Planet. Sci. Lett.* **67**(3), 400–414. https://doi.org/10.1016/0012-821X(84)90178-X.

Miyake A. and Kawano J. (2010) High-temperature molecular dynamics simulation of aragonite. *J. Phys.: Condens. Matter* **22** (22), 225402.

Passey B. H., Levin N. E., Cerling T. E., Brown F. H. and Eiler J. M. (2010) High-temperature environments of human evolution in East Africa based on bond ordering in paleosol carbonates. *Proc. Natl. Acad. Sci.* **107**(25), 11245–11249. https://doi.org/10.1073/pnas.1001824107.

Passey B. H. and Henkes G. A. (2012) Carbonate clumped isotope bond reordering and geospeedometry. *Earth Planet. Sci. Lett.* **351–352**, 223–236. https://doi.org/10.1016/j.epsl.2012.07.021.

Rodríguez-Sanz L., Bernasconi S. M., Marino G., Heslop D., Müller I. A., Fernandez A. and Rohling E. J. (2017) Penultimate deglacial warming across the Mediterranean Sea revealed by clumped isotopes in foraminifera. *Sci. Rep.* **7**(1), 16572. https://doi.org/10.1038/s41598-017-16528-6.

Ryb U. and Eiler J. M. (2018) Oxygen isotope composition of the Phanerozoic ocean and a possible solution to the dolomite problem. *Proc. Natl. Acad. Sci.* **115**(26), 6602–6607. https://doi.org/10.1073/pnas.1719681115.

Ryb U., Lloyd M. K., Stolper D. A. and Eiler J. M. (2017) The clumped-isotope geochemistry of exhumed marbles from Naxos, Greece. *Earth Planet. Sci. Lett.* **470**, 1–12. https://doi.org/10.1016/j.epsl.2017.04.026.

Schauble E. A., Ghosh P. and Eiler J. M. (2006) Preferential formation of ^{13}C–^{18}O bonds in carbonate minerals, estimated using first-principles lattice dynamics. *Geochimica et Cosmochimica Acta* **70**(10), 2510–2529. https://doi.org/10.1016/j.gca.2006.02.011.

Schauer A. J., Kelson J., Saenger C. and Huntington K. W. (2016) Choice of ^{17}O correction affects clumped isotope (Δ_{47}) values of CO_2 measured with mass spectrometry: ^{17}O correction affects CO_2 clumped isotopes. *Rapid Commun. Mass Spectrom.* **30**(24), 2607–2616. https://doi.org/10.1002/rcm.7743.

Shenton B. J., Grossman E. L., Passey B. H., Henkes G. A., Becker T. P., Laya J. C., Perez-Huerta A., Becker S. P. and Lawson M. (2015) Clumped isotope thermometry in deeply buried sedimentary carbonates: The effects of bond reordering and recrystallization. *GSA Bull.* **127**(7–8), 1036–1051. https://doi.org/10.1130/B31169.1.

Staudigel P. T. and Swart P. K. (2016) Isotopic behavior during the aragonite-calcite transition: Implications for sample preparation and proxy interpretation. *Chem. Geol.* **442**, 130–138. https://doi.org/10.1016/j.chemgeo.2016.09.013.

Stolper D. A. and Eiler J. M. (2015) The kinetics of solid-state isotope-exchange reactions for clumped isotopes: A study of inorganic calcites and apatites from natural and experimental samples. *Am. J. Sci.* **315**(5), 363–411.

Thiagarajan N., Adkins J. and Eiler J. (2011) Carbonate clumped isotope thermometry of deep-sea corals and implications for vital effects. *Geochimica et Cosmochimica Acta* **75**(16), 4416–4425. https://doi.org/10.1016/j.gca.2011.05.004.

Thiagarajan N., Subhas A. V., Southon J. R., Eiler J. M. and Adkins J. F. (2014) Abrupt pre-Bølling–Allerød warming and circulation changes in the deep ocean. *Nature* **511**(7507), 75–78. https://doi.org/10.1038/nature13472.

Tripati A. K., Sahany S., Pittman D., Eagle R. A., Neelin J. D., Mitchell J. L. and Beaufort L. (2014) Modern and glacial tropical snowlines controlled by sea surface temperature and atmospheric mixing. *Nat. Geosci.* **7**, 205.

Wang Z., Schauble E. A. and Eiler J. M. (2004) Equilibrium thermodynamics of multiply substituted isotopologues of molecular gases. *Geochim. Cosmochim. Acta* **68**(23), 4779–4797. https://doi.org/10.1016/j.gca.2004.05.039.

Winkelstern I. Z. and Lohmann K. C. (2016) Shallow burial alteration of dolomite and limestone clumped isotope geochemistry. *Geology* **44**(6), 467–470. https://doi.org/10.1130/G37809.1.

Ye Y., Smyth J. R. and Boni P. (2012) Crystal structure and thermal expansion of aragonite-group carbonates by single-crystal X-ray diffraction. *Am. Mineral.* **97**, 707–712. https://doi.org/10.2138/am.2012.3923.

Zhang H., Cai Y., Tan L., Qin S. and An Z. (2014) Stable isotope composition alteration produced by the aragonite-to-calcite transformation in speleothems and implications for paleoclimate reconstructions. *Sed. Geol.* **309**, 1–14. https://doi.org/10.1016/j.sedgeo.2014.05.007.

Associate editor: Miryam Bar-Matthews